General Disclaimer

One or more of the Following Statements may affect this Document

- This document has been reproduced from the best copy furnished by the organizational source. It is being released in the interest of making available as much information as possible.

- This document may contain data, which exceeds the sheet parameters. It was furnished in this condition by the organizational source and is the best copy available.

- This document may contain tone-on-tone or color graphs, charts and/or pictures, which have been reproduced in black and white.

- This document is paginated as submitted by the original source.

- Portions of this document are not fully legible due to the historical nature of some of the material. However, it is the best reproduction available from the original submission.

RELATIVE MOTION CHARACTERISTICS
OF TWO NEAR-EARTH SATELLITES

This report was prepared under

Grant No. NAG5-346

by the

The Center for Space Research
The University of Texas at Austin

Submitted by:

Bob E. Schutz

TABLE OF CONTENTS

ABSTRACT

The stability of the nonlinear dynamical system of two GRAVSAT-type satellites was investigated. The investigation was conducted by performing several numerical experiments which provide the simulations of the relative motions characteristics between the two satellites for various specified time intervals. The simulations include the relative range, range-rate, and the relative acceleration magnitude.

These simulations were generated with respect to appropriate initial orbital elements which were obtained such that the instantaneous separation distance between the two satellites has small fluctuations from a specified constant separation distance. The simulation results indicate that the behavior of the relative motions is very sensitive to the initial orbital elements of the satellites and that for a specified time interval of interest, a stable behavior can only be achieved with the use of an appropriate set of initial orbital elements compatible with the gravity field used to derive them.

PRECEDING PAGE BLANK NOT FILMED
II, III, IV

LIST OF FIGURES

PRECEDING PAGE BLANK NOT FILMED
VI, VII

LIST OF TABLES

CHAPTER 1

INTRODUCTION

Over the past few years, observation of the relative motion between two satellites has gained a potential value for the study of our own planet. There are many geological and geophysical applications such as the study of the structure of the crust and the upper mantle, and accurate determination of the geoid heights in the analysis of the instantaneous and average shape of the sea surface [US National Academy of Sciences, 1979].

In the concept that is currently proposed, the accuracy of the coefficients which describe the gravity field of the earth could be improved by a simple analysis of the direct observations of the relative motions between two low altitude satellites separated by a specified distance in the same near-circular polar orbits. The relative motions which have been suggested for this analysis include range, speed and acceleration magnitude. In addition, the proposal would enable not only improved coefficients, but the determination of a more complete representation of the gravity field, including the anomalous potential.

The history of this concept is attributed to Wolff [1969], who proposed a particular Satellite-to-Satellite Tracking (SST) configuration, known as the "low-low" system. In his proposal the relative speed along the line of sight between two satellites, as a first

approximation, is the difference in anomalous potential sensed by the respective satellites. Therefore, as the Earth rotates, this pair would eventually cover the whole planet with observations of the gravity field. Since this original proposal, research efforts have been directed toward clarifying the theory behind SST.

In the mid 1970's, the idea of a dedicated gravitational satellite mission based on the SST principle began to develop and became known as the Gravity Satellite (GRAVSAT). In order to achieve the mission objective, it is essential that the satellites be made drag-free so that only gravitational forces act upon them. For this reason, a drag-compensation technique has been proposed in which two proof-masses, one inside of each spacecraft, will be unaffected by surface forces through periodic activation of thrusters which would offset the sensed surface forces acting on the spacecraft enclosing the proof-mass. Such a system has been constructed by Stanford University, referred to as the Disturbance Compensation System (DISCOS) [Pisacane et al., 1981]. This drag-compensation system of satellites would be capable of remaining in low altitude orbit for a nominal mission lifetime of up to six months. As long as the drag-compensation mechanism is operable, the atmospheric resistance forces will be effectively eliminated and the satellites will move in orbits governed by gravitational forces. Without such a mechanism, the large drag forces would quickly decay the orbits and make the desired determination of the gravity field far more complicated.

The line of sight measurements between the two satellites would be made by an extremely accurate radar interferometric technique developed at the Applied Physics Laboratory of John Hopkins University [Pisacane et al., 1981]. The range-rate precision is expected to be on the order of ± 1 μm/sec between the two satellites.

The general low-low configuration system along with the desired mission characteristics are shown in Figure 1. The proposed configuration includes a separation of 300 km between the satellites at an altitude of 160 km. Although it is desirable in some cases for the respective satellite orbit planes to coincide, they are illustrated as noncoincident for the general case.

In the following section, descriptions of the major approaches for some of the recent studies, conducted under the use of simplifying assumptions, are presented. These studies provide the motivation for this investigation.

1.1 Motivation for this Study

Basically, an analysis of data for the improvement of geopotential knowledge consists of three major sections, which can be stated as follows:

i. Develop observation equations in order to relate the measurements to the anomalous potential of the Earth.

DIRECTION OF FLIGHT

Separation Distance: 300 km

Satellites Altitude: 160 km

Geocentric Separation Angle
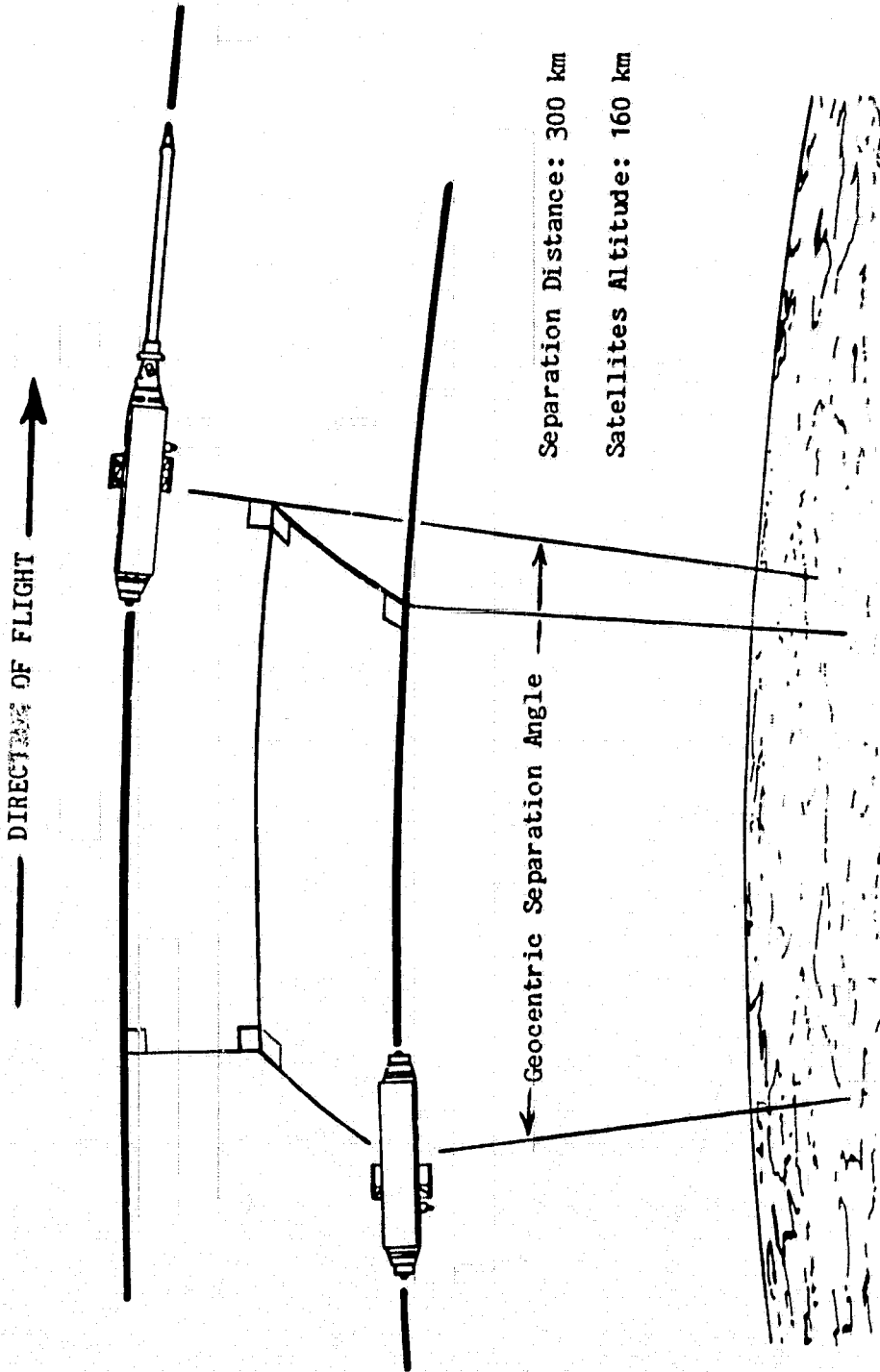
"Low-Low" Configuration of the GRAVSAT System of Satellites

Figure 1

ii. Process the data.

iii. Determine the accuracy of the results.

Of course, the accuracy of the observations and the overall modeling will determine the accuracy of the results.

In general, any globally consistent solution for a degree and order 180 gravity field in terms of spherical harmonic coefficients by least-squares techniques must solve for approximately 32,000 parameters. Consequently, features of the gravity field with 100-200 km in wavelength can be determined [Pisacane and Yionoulis, 1980]. To avoid the massive matrix inversion computations, associated with such a large number of parameters, different methods have been proposed. For example, Colombo [1981] takes advantage of the orthogonality properties with respect to latitude of the spherical harmonics. Also, Kaula [1982] proposed the use of Fourier analysis for each revolution of the satellites.

Some common simplifying assumptions have been made in studies by Colombo [1981], Gaposchkin [1980] and Kaula [1982]. A collection of these assumptions are summarized below:

1. Both satellites describe coplanar, circular, polar orbits with the same geocentric radius.

2. The satellites are separated by a constant distance and the separation distance has small fluctuations.

3.   The plane of the orbits is fixed in inertial   space,   and   fluctua-
     tions in the geocentric angle between the two satellites are small.

These simplifying assumptions lead one to ignore   the   actual   perturba-
tions   of   the   orbits   in the radial, transverse, and normal directions
which are produced due to the effects of the anomalous potential.

The study of the validity of these assumptions and   to   deter-
mine   the extent and rate at which the satellites might drift apart over
various specified time intervals   was   the   primary   objective   of   this
investigation.

1.2 Description of the Present Study

In this study, attention has   been   focused   on   the   relative
motion   of   the satellites, and basically, the stability of this dynamic
system as far as the separation distance was concerned.   To support   The
objective   of   this study, a set of initial orbital elements for each of
the satellites was found so that the instantaneous   separation   distance
(or geocentric separation angle) has small fluctuations from a specified
constant separation distance.   Therefore, a clear prospective of whether
the   stated approximations are valid can be concluded.   A brief descrip-
tion of the material presented in this investigation is   given   as   fol-
lows.

Chapter 2 presents the derivation of the equations   of   motion
considering   only   the   gravitational forces acting upon the satellites.

In addition, a rotating coordinate system attached to the trailing satellite was chosen so that the relative motion between the two satellites can be discussed qualitatively.

Chapter 3 provides the mathematical formulation of an optimization technique used to solve for the initial orbital elements of the satellites. In this method the initial orbital elements of the trailing satellite are specified. Then the orbital elements of the lead satellite are determined such that the relative range between the two satellites is nearly constant over a specified time interval.

Chapter 4 includes the numerical simulations of the relative motions between the two satellites.

Finally, in Chapter 5, based upon the analysis of the numerical simulations, the conclusions of this investigation are summarized.

CHAPTER 2

DYNAMICAL MODEL

This chapter presents the differential equations which describe the motion of two satellites orbiting the Earth under the sole influence of the earth's gravitational field. Section 2.1 includes the gravity field models used in this study. Section 2.2 provides the relationships between the different coordinate systems used in this investigation and the equations of motion are presented in Section 2.3. Section 2.4 provides an analytical definition of the relative range-rate between the two satellites and a satellite-centered coordinate system is introduced. In Section 2.5, an observation equation which relates the line of sight acceleration magnitude and the gravity potentials is obtained such that no simplifying assumptions have been used.

2.1 The Geopotential Models

The gravitational field of the Earth as measured from above its surface can be represented by a potential, U, which satisfies Laplace's equation:

$$\nabla^2 U = 0 \tag{2.1}$$

The solution to Eq. (2.1), using the spherical harmonics representation, is given by the following infinite series [Kaula, 1966]

assuming an origin located at the center of mass:

$$U = \frac{GM}{r}\left[1 - \sum_{n=2}^{N} \left[\frac{a_e}{r}\right]^n J_n P_n(\sin\phi) \right. \tag{2.2}$$

$$\left. + \sum_{n=2}^{N} \sum_{m=1}^{n} \left[\frac{a_e}{r}\right]^n P_{nm}(\sin\phi) \{C_{nm}\cos m\lambda + S_{nm}\sin m\lambda\} \right]$$

where

G = Universal gravitational constant

M = mass of the Earth

a_e = equatorial radius of the Earth

r = radial distance from the center of the Earth

ϕ = geocentric latitude with respect to the equator

λ = angle of longitude with respect to the Greenwich meridian, measured eastward

$P_n(.)$ = Legendre polynomials

$P_{nm}(.)$ = associated Legendre functions

$\left.\begin{array}{c} J_n \\ C_{nm} \\ S_{nm} \end{array}\right\}$ = spherical harmonic coefficients

n = order of the spherical harmonics

m   =   degree of the spherical harmonics

The first term on the right hand side of Eq. (2.2) represents the central body potential and the remaining terms are due to the nonsphericity of the Earth.

Eq. (2.2) is an approximate model of the geopotential where N denotes the truncation order of the geopotential model. For most approximations, N is some finite integer. The spherical harmonic coefficients have been estimated from various data sets. A brief description of some recent determinations are as follows:

- Goddard Earth Model (GEM) 9 [Lerch, et al., 1979] is a gravity model based solely on optical, laser, and electronic observations taken on 30 satellites. It has harmonics complete to degree and order 20 (20x20) with selected higher degree terms.

- GEM-10 [Lerch, et al., 1979] is a combination solution containing a global set of 5 degree surface gravity anomalies along with the data in GEM-9. It has harmonics complete to 22x22 with selected higher degree terms.

- GEM-10B [Lerch, et al., 1981] is a gravity model that combines the GEM-10 data set with those obtained from altimeter data of the GEOS-3 geodetic satellite. GEM-10B represents a significant improvement over GEM-9 and GEM-10. It consists of a field complete to 36x36 in harmonics.

Among the above gravity models, the GEM-9 and GEM-10B were used in the numerical analysis of this investigation.

2.2 Coordinate Systems

Several different coordinate systems were used in the mathematical formulation of the dynamical system for this investigation. Figure 2.1 illustrates these coordinate systems. For simplicity, the precession, nutation, polar motion and changes in rotational speed of the earth have been ignored. The coordinate systems are defined as follows.

The nonrotating, inertially fixed rectangular coordinate system with the origin at the Earth's center of mass denoted by {X,Y,Z}, has the X-axis directed along a fixed direction (e.g., the mean Equinox) and the Y-axis is in the equator. All of the differential equations which describe the motion of the satellites are expressed in this inertial reference system.

A rotating, Earth-fixed rectangular coordinate system with the origin at the Earth's center of mass is present to account for the Earth's rotation and the description of the gravity field coefficients. This system, denoted by {x,y,z}, is a right-handed system with x-y plane coinciding with the equatorial plane of the earth. Therefore, it rotates about the Z-axis with the angular velocity of the Earth. The magnitude of this rotation angle at any instant can be computed by

Figure 2.1

Coordinate Systems
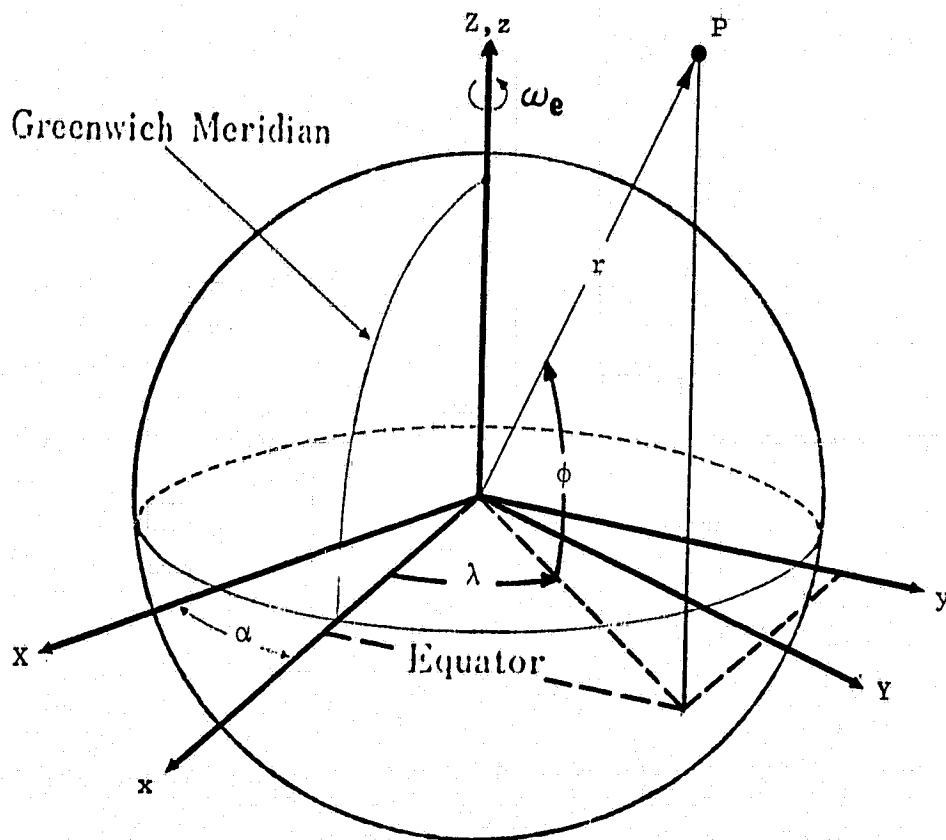
$$\alpha = \alpha_0 + \omega_e (t - t_0) \tag{2.3}$$

where ω_e is the magnitude of the Earth's rotation about the Z-axis, and α_0 is the initial angle at the time t_0. The angle α is measured eastward from the X-axis to the Greenwich meridian. Thus, the components of any vector in the inertial coordinate system can be transformed into the Earth-fixed system by the following transformation matrix:

$$T = \begin{bmatrix} \cos\alpha & \sin\alpha & 0 \\ -\sin\alpha & \cos\alpha & 0 \\ 0 & 0 & 1 \end{bmatrix} \tag{2.4}$$

Of course, T is an orthogonal matrix, therefore the relation $T^{-1} = T^T$ can be used for the inverse transformation.

Finally, the gravitational field of the Earth as defined in Eq. (2.2) is represented in an Earth-centered spherical coordinate system denoted by $\{r,\phi,\lambda\}$. The coordinates of any point on a satellite's orbit in this reference frame is related to the Earth-fixed rotating coordinate system by the following relations:

$$x = r \cos\phi \cos\lambda$$

$$y = r \cos\phi \sin\lambda \tag{2.5}$$

$$z = r \sin\phi$$

where r is the radial distance from the center of mass of the Earth, ϕ is the angle of latitude from the equator, and λ is the angle of longitude measured eastward from the Greenwich meridian.

In addition to the above coordinate systems, a rotating reference frame attached to the trailing satellite is introduced in Section (2.4). This system is used for the theoretical discussion of the relative motion between the two satellites.

2.3 Equations of Motion

In this section, differential equation which describe the relative motion of the two satellites considering only the gravitational forces are presented.

Assume that the mutual gravitational attraction between the two satellites is negligible compared with the earth's gravitational forces acting on them. Therefore, considering the satellites as point masses, the total inertial accelerations of the satellites subject to the Earth's gravitational field are given by

$$\ddot{\bar{R}}_1(t) = \bar{\nabla} U_1(t) \tag{2.6}$$

$$\ddot{\bar{R}}_2(t) = \bar{\nabla} U_2(t) \tag{2.7}$$

where the numerical subscripts 1 and 2 denote the trailing and the lead satellite respectively; $\ddot{\bar{R}}$ is the acceleration vector; $\bar{\nabla}$ is the gradient operator; and U is the gravitational potential of the Earth defined by Eq. (2.2).

Now, with the use of appropriate transformations, the cartesian components of the acceleration of each of the satellites can be

obtained by the following equations:

$$\ddot{X} = \frac{\partial U}{\partial X} \tag{2.8a}$$

$$\ddot{Y} = \frac{\partial U}{\partial Y} \tag{2.8b}$$

$$\ddot{Z} = \frac{\partial U}{\partial Z} \tag{2.8c}$$

The three second-order differential Equations (2.8a) through (2.8c) can be converted to six first-order differential equations as follows:

$$\dot{\overline{R}}(t) = \overline{V}(t) \tag{2.9}$$

$$\dot{\overline{V}}(t) = \nabla U(t) \tag{2.10}$$

where $\overline{R}(t)$ and $\overline{V}(t)$ are the position and velocity vectors, respectively. Given a set of initial components of position (X_o, Y_o, Z_o) and velocity $(\dot{X}_o, \dot{Y}_o, \dot{Z}_o)$ vectors for each of the satellites, Equations (2.9) and (2.10) can be numerically integrated to provide the rectangular components of position (X, Y, Z), and velocity $(\dot{X}, \dot{Y}, \dot{Z})$ vectors at any time for each respective satellite. Then, the relative range vector $(\overline{\rho})$ can be obtained by

$$\overline{\rho} = \overline{R}_2 - \overline{R}_1 \tag{2.11}$$

where the subscripts 1 and 2 denote the trailing and the lead satellite respectively. So, the relative range between the two satellites (ρ) can be computed by

$$\rho = \left[(X_2 - X_1)^2 + (Y_2 - Y_1)^2 + (Z_2 - Z_1)^2 \right]^{1/2} . \tag{2.12}$$

Differentiating Eq. (2.11) twice with respect to time and using Eqs. (2.6) and (2.7) yields

$$\overline{\ddot{\rho}} = \overline{\nabla} U_2 - \overline{\nabla} U_1 \tag{2.13}$$

where $\overline{\ddot{\rho}}$ is the relative acceleration between the two satellites, expressed in the inertial system. Eq. (2.13) is a nonlinear differential equation which describes the relative motion between the two satellites. It should be noted that if the initial orbital elements of the satellites are not chosen properly, an irregularly secular behavior in the separation distance between the two satellites could result.

2.4 Definition of the Relative Range-Rate

The relative velocity vector ($\overline{\dot{\rho}}$) is the time derivative of the relative range vector. Therefore, differentiating Eq. (2.11) yields

$$\overline{\dot{\rho}} = \overline{\dot{R}}_2 - \overline{\dot{R}}_1 \tag{2.14}$$

in the inertial system.

The relative range-rate between the two satellites ($\dot{\rho}$) is mathematically defined as the projection of the relative velocity along the line of sight between the two satellites. In other words, it is the time rate of change in the distance between the two satellites. Accordingly,

$$\dot{\rho} = \hat{\rho} \cdot \overline{\dot{\rho}} = \frac{\overline{\rho} \cdot \overline{\dot{\rho}}}{\|\overline{\rho}\|} \tag{2.15}$$

where $\hat{\rho}$ is a unit vector along the line of sight, and $||\overline{\rho}||$ is the relative range given by Eq. (2.12). Thus, it is of importance to note that $\rho = ||\overline{\rho}||$ but $\dot{\rho}$ is not the same as the magnitude of $\dot{\overline{\rho}}$. Now, by substitution of Eqs. (2.12) and (2.14) in Eq. (2.15), and using the rectangular components of $\dot{\overline{\rho}}$ in the inertial coordinate system, the range-rate can be computed from

$$\dot{\rho} = \frac{(X_2-X_1)(\dot{X}_2-\dot{X}_1) + (Y_2-Y_1)(\dot{Y}_2-\dot{Y}_1) + (Z_2-Z_1)(\dot{Z}_2-\dot{Z}_1)}{\left[(X_2-X_1)^2 + (Y_2-Y_1)^2 + (Z_2-Z_1)^2 \right]^{1/2}} \qquad (2.16)$$

Assume a relative reference frame is attached to the trailing satellite with one axis directed along the line of sight toward the leading satellite as shown in Figure 2.2 (more detail on this reference frame will be given in Section 2.5), then the relative velocity vector in this reference system ($\dot{\overline{\rho}}_r$) can be obtained by

$$\dot{\overline{\rho}}_r = \dot{\overline{\rho}} - \overline{\Omega} \times \overline{\rho} \qquad (2.17)$$

where $\overline{\Omega}$ is the total angular velocity of the satellite-centered rotating coordinate system, and $\dot{\overline{\rho}}$ is the relative velocity vector expressed in the inertial reference frame given by Eq. (2.14). Taking the dot product of $\hat{\rho}$ with Eq. (2.17) results in the following equality:

$$\hat{\rho} \cdot \dot{\overline{\rho}}_r = \hat{\rho} \cdot \dot{\overline{\rho}} = \dot{\rho} \qquad (2.18)$$

since

Figure 2.2

Satellite-Centered Orthogonal Coordinate System
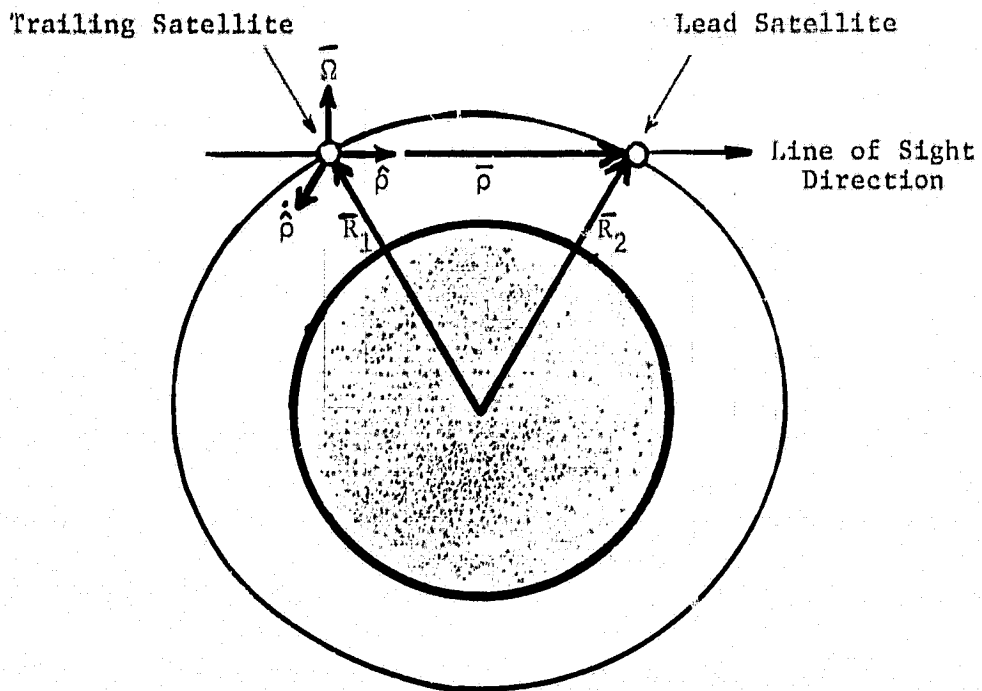
$$\hat{\rho} \cdot (\overline{\Omega} \times \overline{\rho}) = \overline{\Omega} \cdot (\overline{\rho} \times \hat{\rho}) = \overline{0} .$$

Note that Eq. (2.18) yields again the relative range-rate. Therefore, it can be concluded that the relative range-rate can be defined as the projection of the relative velocity in either the inertial or the rotating reference frame along the line of sight.

2.5 Definition of the Relative Acceleration Magnitude

In the following discussion an observation equation is presented in which relative range, relative range-rate, and the line of sight relative acceleration are directly related to the inertial components of the position, velocity, and the acceleration vectors of the satellites. This equation was originally developed by Shao [1982]. In deriving this equation, it should be noted that the line of sight measured quantities are different from the inertial components of the vectors. This equation is of significance due to its generality and that no simplifying assumptions or approximations have been made. In addition, the coordinate system used in the derivation of this equation is identical to the one described in Section 2.4. This choice of reference frame is important because it is inherent to the dynamics of the system, and furthermore the rotation of the lead satellite about the trailing satellite is described by the angular velocity of this reference frame. Further details about the properties of this relative reference frame are given in the following discussion.

The unit vector $\hat{\rho}$ is defined to be a unit vector along the line of sight, so its time rate of change can be obtained from

$$\dot{\hat{\rho}} = \bar{\Omega} \times \hat{\rho} + \dot{\hat{\rho}}_r . \tag{2.19}$$

Since $\hat{\rho}$ is a unit vector, its time derivative in the rotating frame does not change; in other words, $\dot{\hat{\rho}}_r = \bar{0}$. Thus Eq. (2.19) reduces to

$$\dot{\hat{\rho}} = \bar{\Omega} \times \hat{\rho} . \tag{2.20}$$

However, a constant length vector is perpendicular to its time derivative. Therefore,

$$\hat{\rho} \cdot \dot{\hat{\rho}} = 0 \tag{2.21}$$

In addition, by the use of vector algebra equalities, it can be shown that $\dot{\hat{\rho}}$ is perpendicular to $\bar{\Omega}$. The proof is as follows:

$$\dot{\hat{\rho}} \cdot \bar{\Omega} = (\bar{\Omega} \times \hat{\rho}) \cdot \bar{\Omega}$$

$$= \hat{\rho} \cdot (\bar{\Omega} \times \bar{\Omega})$$

Since $\bar{\Omega} \times \bar{\Omega} = 0$, the above equation reduces to

$$\dot{\hat{\rho}} \cdot \bar{\Omega} = 0. \tag{2.22}$$

Equations (2.20), (2.21), and (2.22) represent necessary and sufficient conditions for $\hat{\rho}$, $\dot{\hat{\rho}}$, and $\bar{\Omega}$ to be mutually perpendicular; consequently, they form an orthogonal basis for the previously described

satellite-centered reference frame.

Recall that the relative motion between the two satellites was given by Eq. (2.13) or

$$\ddot{\overline{\rho}} = \overline{\nabla} U_2 - \overline{\nabla} U_1 = \ddot{\overline{R}}_2 - \ddot{\overline{R}}_1 \tag{2.23}$$

where U_1 and U_2 are the potential functions evaluated at the respective satellite positions. Note that the left hand side of Eq. (2.23) is the relative acceleration vector in the inertial coordinate system, and it can also be expressed in the relative reference frame as follows:

$$\ddot{\overline{\rho}} = \frac{d}{dt} (\dot{\overline{\rho}})$$

$$= \frac{d}{dt} (\dot{\overline{\rho}}_r + \overline{\Omega} \times \overline{\rho})$$

$$= (\ddot{\overline{\rho}}_r + \overline{\Omega} \times \dot{\overline{\rho}}_r) + (\dot{\overline{\Omega}} \times \overline{\rho} + \overline{\Omega} \times \dot{\overline{\rho}})$$

Substitute $\dot{\overline{\rho}}_r + \overline{\Omega} \times \overline{\rho}$ for $\dot{\overline{\rho}}$ in the term $\overline{\Omega} \times \dot{\overline{\rho}}$, then it follows that

$$\ddot{\overline{\rho}} = \ddot{\overline{\rho}}_r + 2(\overline{\Omega} \times \dot{\overline{\rho}}_r) - \Omega^2 \overline{\rho} + \dot{\overline{\Omega}} \times \overline{\rho} \tag{2.24}$$

Forming the dot product with $\hat{\rho}$ and both sides of Eq. (2.24) yields

$$\hat{\rho} \cdot \ddot{\overline{\rho}} = \hat{\rho} \cdot \ddot{\overline{\rho}}_r + 2 \hat{\rho} \cdot (\overline{\Omega} \times \dot{\overline{\rho}}_r) \tag{2.25}$$

$$- \hat{\rho} \cdot (\Omega^2 \overline{\rho}) + \hat{\rho} \cdot (\dot{\overline{\Omega}} \times \overline{\rho})$$

Note that each term on the right hand side of Eq. (2.25) simplifies to

$$\hat{\rho} \cdot \overline{\ddot{\rho}}_r = \ddot{\rho} \qquad (2.26a)$$

$$2\,\hat{\rho} \cdot (\,\overline{\Omega} \times \dot{\overline{\rho}}_r\,) = 2\,\overline{\Omega} \cdot (\,\dot{\overline{\rho}}_r \times \overline{\rho}\,) = 0 \qquad (2.26b)$$

$$\hat{\rho} \cdot (\,\Omega^2\,\overline{\rho}\,) = \Omega^2\,\rho \qquad (2.26c)$$

$$\hat{\rho} \cdot (\,\dot{\overline{\Omega}} \times \overline{\rho}\,) = \overline{\Omega} \cdot (\,\overline{\rho} \times \hat{\rho}\,) = 0 \qquad (2.26d)$$

Substitution of Equations (2.26a) through (2.26d) in Eq. (2.25) results in

$$\hat{\rho} \cdot \overline{\ddot{\rho}} = \ddot{\rho} - \Omega^2\,\rho \,. \qquad (2.27)$$

Using Eq. (2.23) and also rearranging the terms, Eq. (2.27) can be written in the form

$$\ddot{\rho} = \Omega^2\,\rho + (\,\overline{\ddot{R}}_2 - \overline{\ddot{R}}_1\,) \cdot \hat{\rho}$$

or

$$\ddot{\rho} = \Omega^2\,\rho + (\,\overline{\nabla}\,U_2 - \overline{\nabla}\,U_1\,) \cdot \hat{\rho} \qquad (2.28)$$

Eq. (2.28) is the observation equation where $\ddot{\rho}$ is the line of sight relative acceleration, ρ is the relative range, and Ω is the magnitude of the angular velocity of the rotating relative reference frame, which can be computed in terms of inertial components of position and velocity of the two satellites as follows.

Taking the cross product of $\hat{\rho}$ with both sides of Eq. (2.20) yields

$$\hat{\rho} \times \dot{\hat{\rho}} = \hat{\rho} \times (\bar{\Omega} \times \hat{\rho}). \tag{2.29}$$

Using the following vector algebra equality

$$\bar{A} \times (\bar{B} \times \bar{C}) = \bar{B}(\bar{A} \cdot \bar{C}) - \bar{C}(\bar{A} \cdot \bar{B})$$

then Eq. (2.29) can be written as

$$\hat{\rho} \times \dot{\hat{\rho}} = \bar{\Omega} (\hat{\rho} \times \hat{\rho}) - \hat{\rho} (\hat{\rho} \cdot \bar{\Omega}). \tag{2.30}$$

Since $\hat{\rho}$ is perpendicular to $\bar{\Omega}$, Eq. (2.30) reduces to

$$\hat{\rho} \times \dot{\hat{\rho}} = \bar{\Omega} . \tag{2.31}$$

Therefore, $\bar{\Omega}$ is defined by Eq. (2.31), and Ω^2 can be computed from

$$\Omega^2 = \| \hat{\rho} \times \dot{\hat{\rho}} \|^2$$

$$= (\hat{\rho} \times \dot{\hat{\rho}}) \cdot (\hat{\rho} \times \dot{\hat{\rho}}) \tag{2.32}$$

Using the following vector algebra equality

$$(\bar{A} \times \bar{B}) \cdot (\bar{C} \times \bar{D}) = (\bar{A} \cdot \bar{C})(\bar{B} \cdot \bar{D}) - (\bar{A} \cdot \bar{D})(\bar{B} \cdot \bar{C})$$

then Eq. (2.32) can be rewritten in the form of

$$\Omega^2 = (\hat{\rho} \cdot \hat{\rho})(\dot{\hat{\rho}} \cdot \dot{\hat{\rho}}) - (\hat{\rho} \cdot \dot{\hat{\rho}})(\hat{\rho} \cdot \dot{\hat{\rho}}) \tag{2.33}$$

Note that $\dot{\hat{\rho}}$ is perpendicular to $\hat{\rho}$, thus $\dot{\hat{\rho}} \cdot \hat{\rho} = 0$. Then, Eq. (2.33) reduces to

$$\Omega^2 = \dot{\hat{\rho}} \cdot \dot{\hat{\rho}} = (\dot{\hat{\rho}})^2 . \tag{2.34}$$

$\dot{\hat{\rho}}$ is the time rate of change of $\hat{\rho}$, and can be obtained as follows

$$\dot{\hat{\rho}} = \frac{d}{dt} (\hat{\rho})$$

$$= \frac{d}{dt} (\frac{\bar{\rho}}{\rho})$$

$$= \frac{\rho \dot{\bar{\rho}} - \dot{\rho} \bar{\rho}}{\rho^2} \tag{2.35}$$

Finally, Ω^2 can be computed by substitution of $\dot{\hat{\rho}}$ in Eq. (2.34), as follows:

$$\Omega^2 = \left[\frac{\rho \dot{\bar{\rho}} - \dot{\rho} \bar{\rho}}{\rho^2} \right]^2$$

$$= \frac{1}{\rho^4} \left[\rho^2 (\dot{\bar{\rho}})^2 - 2 \rho^2 \dot{\rho}^2 + \rho^2 \dot{\rho}^2 \right]$$

$$= \frac{1}{\rho^2} \left[(\dot{\bar{\rho}})^2 - \dot{\rho}^2 \right] \tag{2.36}$$

where $\dot{\rho}$ is the relative range-rate given by Eq. (2.16), and

$$(\dot{\bar{\rho}})^2 = (\dot{X}_2 - \dot{X}_1)^2 + (\dot{Y}_2 - \dot{Y}_1)^2 + (\dot{Z}_2 - \dot{Z}_1)^2 .$$

Note that $\overline{\Omega}$ in general is time dependent and a function of position and velocity of the satellites. And in particular, if the coplanarity, circularity, and constant relative separation orbital assumptions are made, then $\overline{\Omega}$ would be constant with a fixed direction perpendicular to the orbital plane.

Now, using Eq. (2.36) for substitution of Ω^2 in Eq. (2.28), then $\ddot{\rho}$ can be obtained in terms of the rectangular components of the position, velocity, and acceleration of the satellites in the fixed coordinate system as follows:

$$\ddot{\rho} = \frac{1}{\rho}\left[(\dot{\overline{\rho}})^2 - \dot{\rho}^2 \right] + (\overline{\nabla} U_2 - \overline{\nabla} U_1) \cdot \hat{\rho} \tag{2.37a}$$

$$\ddot{\rho} = \frac{1}{\rho}\left[(\dot{\overline{\rho}})^2 - \dot{\rho}^2 \right] + (\ddot{\overline{\rho}}) \cdot \hat{\rho} \tag{2.37b}$$

$$\ddot{\rho} = \frac{1}{\rho}\left[(\dot{\overline{\rho}})^2 - \dot{\rho}^2 + \ddot{\overline{\rho}} \cdot \overline{\rho} \right] \tag{2.37c}$$

$$\ddot{\rho} = \frac{1}{\rho}\left[(\dot{X}_2-\dot{X}_1)^2 + (\dot{Y}_2-\dot{Y}_1)^2 + (\dot{Z}_2-\dot{Z}_1)^2 - \dot{\rho}^2 \right.$$
$$\left. + (X_2-X_1)(\ddot{X}_2-\ddot{X}_1) + (Y_2-Y_1)(\ddot{Y}_2-\ddot{Y}_1) + (Z_2-Z_1)(\ddot{Z}_2-\ddot{Z}_1) \right] \tag{2.37d}$$

From any of the above equations, it can be concluded that the line of sight relative acceleration is different from the magnitude of the relative inertial acceleration. Furthermore, their difference is not a constant quantity.

In summary, the set of equations required to calculate the relative motions between the two satellites are as follows. The state of each of the satellites is calculated by integration of Eqs. (2.9) and (2.10) for the respective satellite. Then, the relative range is computed by Eq. (2.12), the relative range-rate by Eq. (2.16), and the relative acceleration magnitude by Eq. (2.37d).

CHAPTER 3

DETERMINATION OF APPROPRIATE INITIAL ORBITAL ELEMENTS

In the previous chapter, it was shown that the relative motion between the two satellites is governed by the nonlinear accelerations produced due to the earth's gravitational field.

The stability of the present nonlinear dynamical system has a direct dependency on the initial orbital elements of the satellites. As it will shown in Chapter 4, a simple numerical simulation of the relative range between the two satellites, with any arbitrarily selected initial conditions, will illustrate a secular behavior in the separation distance with oscillations of large amplitude. Therefore, in order to obtain a stable behavior in the relative motion, and to maintain small fluctuations between the two satellites, a method is developed to obtain appropriate initial orbital elements. In this method, the initial orbital elements of one of the satellites is specified. Then, using the principle of least squares, the initial orbital elements of the other satellite are numerically obtained to minimize the sum of the squares of the changes in the separation distance from a desired constant distance. The formulation of this problem is presented in Section 3.1, and the solution is obtained by using an iterative method which is introduced in Section 3.2. Finally, a computational algorithm is summarized in Section 3.3.

3.1 Problem Formulation

Having described the dynamical system represented by the system of Eqs. (2.6) and (2.7), the differential equations describing the state (position and velocity) of the satellites, $\bar{X}_1$ and $\bar{X}_2$, can be written in the form of

$$\dot{\bar{X}}_1(t) = \bar{F}_1(\bar{X}_1, t) \qquad (3.1)$$

$$\dot{\bar{X}}_2(t) = \bar{F}_2(\bar{X}_2, t) \qquad (3.2)$$

where $\bar{F}_1(.)$ and $\bar{F}_2(.)$ are nonlinear functions of $\bar{X}_1$ and $\bar{X}_2$ respectively.

Let the initial components of position and velocity of one of the satellites, say the trailing satellite, be fixed and denoted by $\bar{X}_{1_o}$. Then, it is desired to solve for the appropriate initial components of the position and velocity of the lead satellite as arranged in the estimation state vector

$$\bar{X}_{2_o} = \left[X_{2_o} \quad Y_{2_o} \quad Z_{2_o} \quad \dot{X}_{2_o} \quad \dot{Y}_{2_o} \quad \dot{Z}_{2_o} \right]^T \qquad (3.3)$$

Let ρ_c be the desired constant separation distance between the two satellites. Then, at any instant of time t during a specified time interval, the change in the separation distance is defined by

$$r = \rho - \rho_c \qquad (3.4)$$

where ρ is the relative range which can be computed by Eq. (2.12) and r

is referred to as the residual.

The optimal solution is obtained by solving a deterministic optimization problem for which the performance index is the sum of the square of the residuals. In this approach, the commonly defined performance index can be expressed as

$$P = \int_{t_o}^{t_f} \{ r^2 \} \, dt \tag{3.5}$$

where

P = the function to be minimized

t_o = the initial time

t_f = the specified final time

First variations of P with respect to the components of the estimation state vector are obtained by

$$\left[\frac{\partial P}{\partial \overline{X}_{2_o}} \right] = \int_{t_o}^{t_f} \left\{ 2 \left[\frac{\partial r}{\partial \overline{X}_{2_o}} \right]^T r \right\} \, dt \tag{3.6}$$

In order to minimize P, first variations of P must vanish. Hence, six nonlinear equations are produced which are

$$\int_{t_o}^{t_f} \left\{ \left[\frac{\partial \rho}{\partial X_{2_o}} \right] r \right\} \, dt = 0 \tag{3.7a}$$

$$\int_{t_o}^{t_f} \left\{ \left[\frac{\partial \rho}{\partial Y_{2_o}} \right] r \right\} \, dt = 0 \tag{3.7b}$$

$$\int_{t_o}^{t_f} \left\{ \left[\frac{\partial \rho}{\partial Z_{2_o}} \right] r \right\} dt = 0 \qquad (3.7c)$$

$$\int_{t_o}^{t_f} \left\{ \left[\frac{\partial \rho}{\partial \dot{X}_{2_o}} \right] r \right\} dt = 0 \qquad (3.7d)$$

$$\int_{t_o}^{t_f} \left\{ \left[\frac{\partial \rho}{\partial \dot{Y}_{2_o}} \right] r \right\} dt = 0 \qquad (3.7e)$$

$$\int_{t_o}^{t_f} \left\{ \left[\frac{\partial \rho}{\partial \dot{Z}_{2_o}} \right] r \right\} dt = 0 \qquad (3.7f)$$

Equations (3.7a) through (3.7f) can be put in a matrix form as follows:

$$\bar{f} = \int_{t_o}^{t_f} \left\{ \left[\frac{\partial \rho}{\partial \bar{X}_{2_o}} \right]^T r \right\} dt = \bar{0} \qquad (3.8)$$

and if the following definition is introduced,

$$H = \left[\frac{\partial \rho}{\partial \bar{X}_{2_o}} \right] \qquad (3.9)$$

Eq. (3.8) then can be expressed in terms of H matrix by

$$\bar{f} = \int_{t_o}^{t_f} \left\{ H^T r \right\} dt = \bar{0} . \qquad (3.10)$$

Thus, the problem reduces to solving the six nonlinear equations of $\overline{f}$ in terms of six unknown components of the estimation state vector of $\overline{X}_{2_o}$.

3.2 Solution Method

A very frequent computational problem is to find some or all of the solutions of a system of n simultaneous nonlinear equations. One approach to solve such system of equations is to generalize to n dimensions one of the iterative processes used for solving a single equation; see for instance Forsythe, et al. [1977]. There are several methods available from which the system of equations defined by Eq. (3.10) can be solved. However, the Newton-Raphson iterative method was chosen and the solution is obtained as follows.

Assume that the partial derivatives of the functions f_i with respect to the components of $\overline{X}_{2_o}$ can all be computed. Then, let $J(\overline{X}_{2_o})$ represent the Jacobian matrix whose (i,j)th element is defined by

$$J_{ij}(\overline{X}_{2_o}) = \frac{\partial f_i}{\partial X_{2_{o_j}}} \tag{3.11}$$

As in the case of one dimension, the Newton idea is to start with an arbitrary $\overline{X}_{2_o}$, say $\overline{X}_{2_o}^o$. Then, the function $\overline{f}$ can be linearized at $\overline{X}_{2_o}^o$ by expanding $\overline{f}$ into a Taylor series which by using the above definition it can be written in the form of

$$\overline{f}(\overline{X}_{2_o}) = \overline{f}(\overline{X}_{2_o}^o) + J(\overline{X}_{2_o}^o)(\overline{X}_{2_o} - \overline{X}_{2_o}^o) + \ldots \tag{3.12}$$

Now, keeping only the terms of degree 0 and 1, the first approximation to the solution of Eq. (3.10) can be obtained by solving the following equation for $\overline{X}_{2_o}$:

$$\overline{f}(\overline{X}^o_{2_o}) + J(\overline{X}^o_{2_o}) \, (\overline{X}_{2_o} - \overline{X}^o_{2_o}) = \overline{0} \tag{3.13}$$

and the first approximate solution $\overline{X}_{2_o} = \overline{X}^1_{2_o}$ is obtained which is:

$$\overline{X}^1_{2_o} = \overline{X}^o_{2_o} - J^{-1}(\overline{X}^o_{2_o}) \quad \overline{f}(\overline{X}^o_{2_o})$$

Of course, in the general step of the iteration, if $\overline{X}^k_{2_o}$ is the solution obtained at the kth iteration, the next approximation to the solution can be computed by

$$\overline{X}^{k+1}_{2_o} = \overline{X}^k_{2_o} - J^{-1}(\overline{X}_{2_o}) \Big|_{\overline{X}^k_{2_o}} \overline{f}(\overline{X}_{2_o}) \Big|_{\overline{X}^k_{2_o}} \tag{3.14}$$

Note that the second term on the right hand side of Eq. (3.14) represents the correction to the approximate initial state of the lead satellite. And if the correction at each iteration is denoted by $\overline{\delta}(\overline{X}^k_{2_o})$ then Eq. (3.14) can be written in the form of:

$$\overline{X}^{k+1}_{2_o} = \overline{X}^k_{2_o} - \overline{\delta}(\overline{X}^k_{2_o}) \tag{3.15}$$

where

$$\overline{\delta}(\overline{X}^k_{2_o}) = J^{-1}(\overline{X}_{2_o}) \Big|_{\overline{X}^k_{2_o}} \overline{f}(\overline{X}_{2_o}) \Big|_{\overline{X}^k_{2_o}} \tag{3.16}$$

Existence of the Solution

Convergence of the solution using Newton's method depends on the initial guess of the state vector which is required to start the iteration process. In other words, suppose $\bar{X}_{2_0}^*$ is a nominal solution of $\bar{f} = \bar{0}$. Then, if the initial guess $(\bar{X}_{2_0}^0)$ is sufficiently "close" to $\bar{X}_{2_0}^*$, the Newton iteration will converge, and

$$\bar{X}_{2_0}^k \rightarrow \bar{X}_{2_0}^* \quad \text{as} \quad k \rightarrow \infty$$

Moreover, high-speed convergence will start when $\bar{X}_{2_0}^k$ gets sufficiently close to $\bar{X}_{2_0}^*$. Although, it should be noted that as soon as the difference between the obtained solution at the kth iteration and the nominal solution defined by

$$\bar{e}^k = \bar{X}_{2_0}^k - \bar{X}_{2_0}^*$$

reaches to the order of the distance between nearby floating point numbers, the granular structure of the number system makes it no longer possible to continue the iteration.

The other criteria which should also be satisfied at each iteration is that the Jacobian matrix be non-singular so that it can be converted in order to compute the correction $\bar{\delta}(\bar{X}_{2_0}^k)$.

Computation of the Jacobian Matrix (J)

The Jacobian matrix (6x6) was defined by Eq. (3.11) and can be computed as follows. Using Eq. (3.8) for substitution of T into Eq. (3.11), it then follows:

$$J(\overline{X}_{2_o}) = \frac{\partial}{\partial \overline{X}_{2_o}} \left[\int_{t_o}^{t_f} \left\{ \left[\frac{\partial \rho}{\partial \overline{X}_{2_o}} \right]^T r \right\} dt \right] \tag{3.17a}$$

$$= \int_{t_o}^{t_f} \left\{ \frac{\partial}{\partial \overline{X}_{2_o}} \left[\left[\frac{\partial \rho}{\partial \overline{X}_{2_o}} \right]^T \right] r \right\} dt \tag{3.17b}$$

$$+ \int_{t_o}^{t_f} \left\{ \left[\frac{\partial \rho}{\partial \overline{X}_{2_o}} \right]^T \left[\frac{\partial \rho}{\partial \overline{X}_{2_o}} \right] \right\} dt$$

Neglecting the small terms (second partial derivatives of ρ with respect to the components of $\overline{X}_{2_o}$) which are associated with the first term on the right hand side of Eq. (3.17b), and also using the definition of Eq. (3.9), $J(\overline{X}_{2_o})$ can then be computed approximately by

$$J(\overline{X}_{2_o}) \simeq \int_{t_o}^{t_f} \left\{ H^T H \right\} dt \tag{3.18}$$

J is a symmetric matrix and along with T in Eq. (3.10), both are expressed in terms of H which can be obtained as in the following.

Computation of H Matrix

The components of the H matrix (1x6) are not an explicit function of the components of $\overline{X}_{2_o}$. Therefore, using the chain rule, the H matrix can be written in the form of

$$H = \left[\frac{\partial \rho}{\partial \overline{X}_{2_o}}\right] = \left[\frac{\partial \rho}{\partial \overline{X}_2}\right] \left[\frac{\partial \overline{X}_2}{\partial \overline{X}_{2_o}}\right] \tag{3.19}$$

And, if the following definitions are introduced,

$$\tilde{H} = \left[\frac{\partial \rho}{\partial \overline{X}_2}\right] \tag{3.20}$$

$$\Phi(t,t_o) = \left[\frac{\partial \overline{X}_2}{\partial \overline{X}_{2_o}}\right] \tag{3.21}$$

then Eq. (3.19) can be expressed in terms of $\tilde{H}$, and ϕ as

$$H = \tilde{H}\phi \tag{3.22}$$

Components of the $\tilde{H}$ matrix can be obtained by taking the partial derivatives of ρ, defined by Eq. (2.12), with respect to the components of the state of the lead satellite $\overline{X}_2$ at some instance of time.

These partials are:

$$\frac{\partial \rho}{\partial X_2} = \frac{X_2 - X_1}{\rho} \tag{3.23a}$$

$$\frac{\partial \rho}{\partial Y_2} = \frac{Y_2 - Y_1}{\rho} \tag{3.23b}$$

$$\frac{\partial \rho}{\partial Z_2} = \frac{Z_2 - Z_1}{\rho} \tag{3.23c}$$

$$\frac{\partial \rho}{\partial \dot{X}_2} = 0 \tag{3.23d}$$

$$\frac{\partial \rho}{\partial \dot{Y}_2} = 0 \tag{3.23c}$$

$$\frac{\partial \rho}{\partial \dot{Z}_2} = 0 \tag{3.23e}$$

Collecting the partials from Eqs. (3.23a) through (3.23e), the $\tilde{H}$ matrix is then computed by

$$\tilde{H} = \left[\frac{X_2 - X_1}{\rho} \quad \frac{Y_2 - Y_1}{\rho} \quad \frac{Z_2 - Z_1}{\rho} \quad 0 \quad 0 \quad 0 \right] \tag{3.24}$$

The State Transition Matrix

The state transition matrix, ϕ, is defined by Eq. (3.21). Based on Eq. (3.2) which represented the nonlinear dynamics of the lead satellite, assuming that $\overline{X}_2^*(t)$ is a nominal solution of Eq. (3.2), then the deviation of $\overline{X}_2^*$ from the "true" solution $\overline{X}_2(t)$ at any instance of time is defined by

$$\bar{X}_2(t) = \bar{X}_2(t) - \bar{X}_2^*(t)$$

Furthermore, assuming that $\bar{X}_2^*(t)$ is sufficiently "close" to $\bar{X}_2(t)$, then the function $\bar{F}_2$ can be linearized about $\bar{X}_2^*$ by expanding $\bar{F}_2$ into a Taylor series. Keeping only the terms of degree 0 and 1, and provided that $A(t)$ matrix is obtained from $\bar{F}_2(.)$ by the following definition:

$$A(t) = \left. \frac{\partial \bar{F}_2}{\partial \bar{X}_2} \right|_{\bar{X}_2^*} \tag{3.25}$$

then it can be shown that the following linear system of equations are satisfied [Brogan, 1974]:

$$\dot{\bar{X}}_2(t) = A(t) \, \bar{X}_2(t) \tag{3.26}$$

and that the state transition matrix satisfies the following differential equations:

$$\dot{\Phi}(t,t_o) = A(t) \, \Phi(t,t_o) \, , \qquad \Phi(t_o,t_o) = I \tag{3.27}$$

where I is an identity matrix. Thus, the state transition matrix can be computed by numerical integration of Eq. (3.27) from t_o up to t.

Summarizing, in order to minimize the performance index defined by Eq. (3.5), the following differential equations need to be simultaneously integrated to result in the appropriate initial orbital elements of the lead satellite:

- Six equations of motion for the trailing satellite given by

$$\dot{\overline{X}}_1 = \overline{F}_1 \quad , \qquad \overline{X}_1(t_o) = \overline{X}_{1_o} \tag{3.28}$$

- Six equations of motion for the lead satellite given by

$$\dot{\overline{X}}_2 = \overline{F}_2 \quad , \qquad \overline{X}_2(t_o) = \overline{X}_{2_o} \tag{3.29}$$

- Six equations for the elements of 6x1 function $\overline{f}$ given by

$$\dot{\overline{f}} = H^T r \quad , \qquad \overline{f}(t_o) = \overline{0} \tag{3.30}$$

- Thirty-six equations for the elements of the 6x6 Jacobian matrix given by

$$\dot{J} = H^T H \quad , \qquad J(t_o) = 0 \tag{3.31}$$

- Thirty-six equations for the elements of the 6x6 state transition matrix given by

$$\dot{\Phi} = A \Phi \quad , \qquad \Phi(t_o, t_o) = I \tag{3.32}$$

- One optional equation may also be integrated to determine the effect of the convergence of the solution on the value of the performance index which can be computed by integrating the following differential equation:

$$\dot{P} = r^2 \quad , \qquad P(t_o) = 0 \tag{3.33}$$

3.3 Computation Algorithm

In this section a batch type computational algorithm [Tapley, 1973] is presented which requires the integration of 91 first-order differential equations summarized by Eqs. (3.28) through (3.33). The following steps lead to the iteration process of the estimation of the appropriate initial orbital elements for the lead satellite, $\overline{X}_{2_o}^*$.

0. Initialize the state vectors, $\overline{X}_1(t_o) = \overline{X}_{1_o}$ and $\overline{X}_2(t_o) = \overline{X}_{2_o}^0$. Set ρ_c to the desired constant separation distance.

1. Set the iteration number k=1 and $\overline{X}_{2_o}^k = \overline{X}_{2_o}^0$.

2. Initialize the matrices, (6x1) $\overline{f}=0$, (6x6) $J=0$, (6x6) $\Phi=I$, and P=0.

3. Set i=1 and $t_i = t_o$.

4. Compute the A matrix at t_i.

5. Compute the $\widetilde{H}$ matrix at t_i.

6. Compute the $H = \widetilde{H} \Phi$.

7. Compute $r = \left|\left| \overline{X}_2^k(t_i) - \overline{X}_1^k(t_i) \right|\right| - \rho_c$.

8. Increment time: $t_i = t_i + \Delta t$.

9. Check: if $t_i > t_f$, then go to Step 10. Otherwise,

- Integrate the equations of motion to get $\overline{X}_1^k(t_i)$, and $\overline{X}_2^k(t_i)$.

- Integrate the state transition matrix to get Φ at t_i.

- Integrate $\dot{\overline{r}} = H^T r$.

- Integrate $\dot{J} = H^T H$.

- Integrate the performance index, $\dot{P} = r^2$ (optional).

- Go to Step 4.

10. Compute the correction $\overline{\delta}^k$ at t_f, $\overline{\delta}^k = J^{-1} \overline{r}$.

11. Compute $\overline{X}_{2_o}^{k+1} = \overline{X}_{2_o}^k - \overline{\delta}^k$.

12. Check the convergence. If $\left|\left|\overline{\delta}^k\right|\right| >$ tolerance, then:

    - Increment k: $k = k+1$.

    - Replace $\overline{X}_{2_o}^k$ by $\overline{X}_{2_o}^{k+1}$, go to Step 2 for the next iteration.

13. Otherwise, the final approximate solution $\overline{X}_{2_o}^*$ is obtained which is the same as $\overline{X}_{2_o}^{k+1}$.

CHAPTER 4

SIMULATIONS OF THE RELATIVE MOTIONS

In this chapter, the relative motion characteristics between two GRAVSAT type satellites have been numerically investigated. The investigation includes the analysis of the changes in the relative motions produced due to the effects of the earth's gravity field models which were described in Section 2.1.

Several numerical experiments were performed in order to provide the simulations of the relative motions which are the relative range, range-rate, and acceleration magnitude. The equations used to compute the relative motions were derived in Chapter 2, where they are given by Eqs. (2.12), (2.16), and (2.37d), respectively.

The estimation algorithm which was developed in Section 3.3 has been used extensively to obtain the appropriate initial orbital elements of the lead satellite for several different time intervals. The software program developed to perform the numerical experiments is briefly described in Section 4.1.

The constant parameters and the set of initial orbital elements of the trailing satellite which are held constant throughout the simulations are specified in Section 4.2.

41

The other sections of this chapter are devoted to the objectives of this investigation which are as follows:

1. To establish a stable behavior in the relative motions under the influence of GEM-10B gravity field model (see Section 4.3).

2. To determine the variations in the relative motion produced due to the effect of slight changes in the second degree zonal harmonic coefficient of the GEM-10B gravity field model (see Section 4.4).

3. To determine the level of variations produced due to the effects of gravity field model error which is assumed to be the difference between the GEM-10B and the GEM-9 models (see Section 4.5.)

The first objective is directly related to the investigation of the "stability" of the separation distance between the two satellites, wherein the GEM-10B gravity field model is assumed to represent the "best" approximate model representing the earth's gravitational field.

The second and the third objectives are investigated in connection with the fact that in the actual mission the satellites would sense the real effects of the earth's gravitational field which are expected to differ from the effects resulting from the a priori model. Therefore, it has been attempted to demonstrate the variations in the relative motions which would be "similar" to those in the actual mission.

4.1 Software Description

The software created to perform the numerical experiments of this investigation was designed to be implemented on the Control Data Corporation (CDC) Dual Cyber 170/750 computer system. The primary objective of the program was to perform the numerical optimization of the problem discussed in Chapter 3. Various software packages were also incorporated which were developed at the University of Texas at Austin. For example, the normalized harmonic coefficients of the geopotential expansion were processed by routines of UTOPIA (University of Texas Orbit Processor Incorporating Statistical Analysis) developed by Schutz and Tapley [1980], and the numerical integration of the equations of motion and the other differential equations required for the optimization algorithm were performed by using the DELIB software package written by McKenzie [1978].

DELIB is a collection of six separate integration packages useful for the numerical solution of ordinary differential equations. Two of these integration packages are called ODE and ABFS, which are useful for solving a system of first-order differential equations. ODE uses the variable-mesh multistep method of Shampine and Gordon [1975], whereas ABFS uses fixed-order, fixed-mesh Adams method developed by Lundberg [1981]. The results of the numerical integrations using the ODE package were more accurate compared with the use of the ABFS package. However, the computation time efficiency was greatly improved by the use of the ABFS package due to the fixed-step Adams method with

minimal overhead cost. In addition, both of the packages use the PECE (Predict Evaluate Correct Evaluate) technique where two function evaluations are made at each integration time step. Therefore, a remarkable computer execution time efficiency was also achieved by the use of psuedo function evaluations where only the two-body and the second degree zonal harmonic contributions to the accelerations of the satellites were reevaluated when the second function evaluation of the PECE technique was made.

4.2 General Specifications

In the numerical simulations, there were several parameters which, for simplicity, were held constant. These parameters are:

1. The epoch time (t_o) and the angle of longitude of the Greenwich Meridian (α) at epoch which were set to be equal to zero. Hence, all of the simulations are generated with respect to,

$$t_o = 0, \text{ and}$$

$$\alpha_o = 0.$$

2. The constants which describe the physical and dynamical characteristics of the earth are specified in Table 4.1; wherein, R_e is the equatorial radius, GM is the gravitational coefficient, and ω_e is the mean magnitude of the earth's rotation about the Z-axis.

Initial Orbital Elements of the Trailing Satellite

The particular set of initial orbital elements of the trailing satellite which are used for all of the numerical simulations are chosen according to the configuration which is shown in Figure 4.1. This configuration suggests that the trailing satellite starts from the ascending node of its orbit which is located at the altitude (h) of 160 kilometers on the X-axis. The initial circular speed assigned to the satellite is computed as follows

$$V = \left[\frac{GM}{R_e + h} \right]^{1/2} = 7808.034 \ \text{m/sec.}$$

The respective initial orbital elements (Keplerian or the inertial components of the position and velocity) are computed which are given in Table 4.2. These initial orbital elements of the trailing satellite are held constant regardless of the various time intervals, for which the simulations are generated.
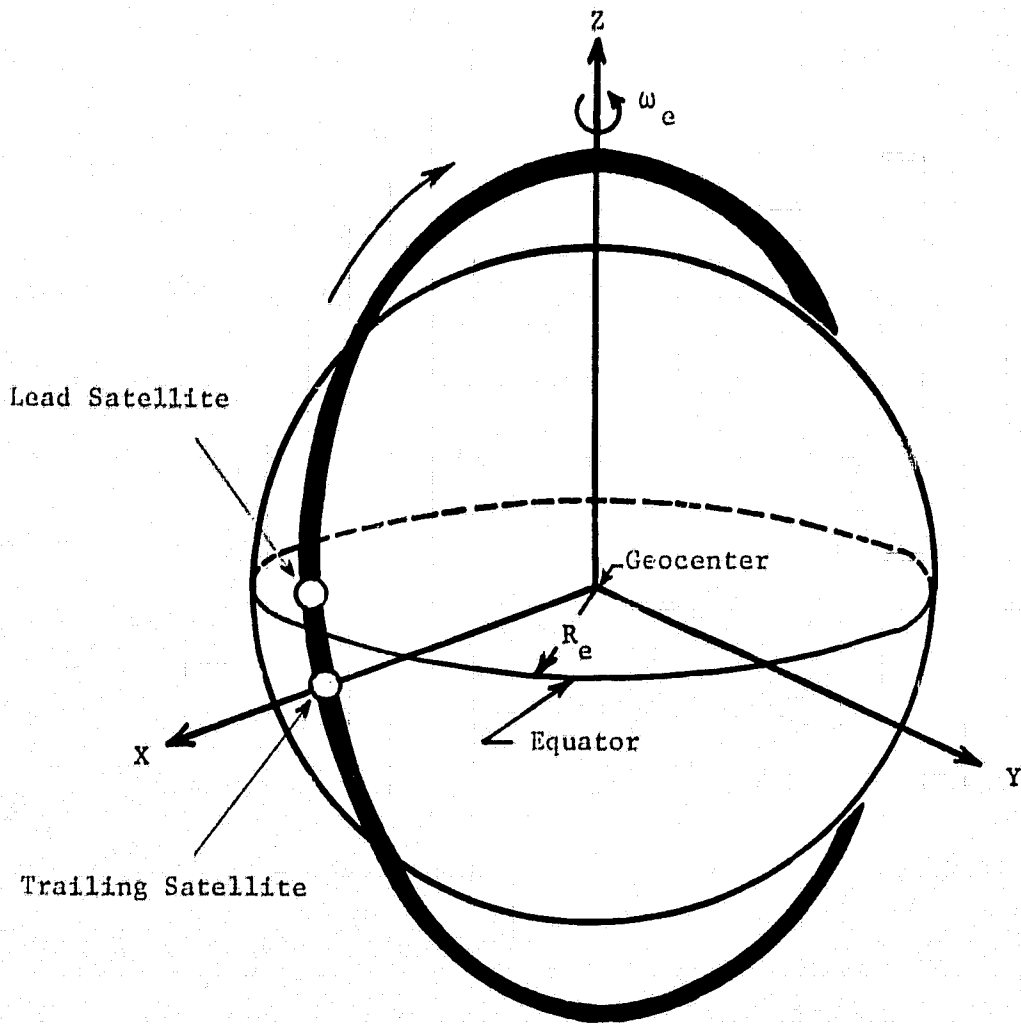
Figure 4.1

Dynamics Profile

Table 4.1

Constants of the Earth

GM (m^3/sec^2)	=	0.39860064 E+15
R_e (m)	=	6378145.0
ω_e (rad/sec)	=	0.72921151 E-04

Table 4.2

Initial Orbital Elements of the Trailing Satellite
Used for all of the Numerical Simulations

Inertial Rectangular Orbital Elements			Keplerian[*] Orbital Elements		
X (m)	=	6538145.000	a (m)	=	R_e + 160000.0
Y (m)	=	0.0	e	=	0.0
Z (m)	=	0.0	i (deg)	=	90.0
$\dot{X}$ (m/s)	=	0.0	ω (deg)	=	0.0
$\dot{Y}$ (m/s)	=	0.0	Ω (deg)	=	0.0
$\dot{Z}$ (m/s)	=	7808.034	M (deg)	=	0.0

[*] Keplerian orbital elements are defined by:

    a = Semi-major axis

    e = Eccentricity

    i = Inclination

    ω = Argument of perigee

    Ω = Longitude of node

    M = Mean anomaly

4.3 General Behavior of the Relative Motions Characteristics

The behavior of the relative motions between the two satellites is generally dependent on the initial orbital elements of the satellites. In this section, it is attempted to establish a stable behavior in the relative motions for a 12-day arc length, or time interval. All of the relative motion simulations are obtained with the use of the GEM-10B gravity field model which has harmonics complete to degree and order 36. The numerical experiments which are performed to provide the simulations are as follows.

A set of initial orbital elements for the lead satellite are chosen such that both of the satellites are located in the same orbital plane with equal circular speeds and radial distances from the center of the earth. Thus, having specified the initial orbital elements of the trailing satellite, the same initial orbital elements are used for the lead satellite except for a mean anomaly difference of 2.629 degrees which gives approximately an initial separation distance of 300 kilometers. The respective inertial components of the position and velocity of the lead satellite as computed are given in Table 4.3. Using these initial set of orbital elements, the equations of motion for each of the satellites are numerically integrated to generate the simulations of the relative motions for a 1-day arc length which are plotted as shown in Figures 4.2a through 4.2c (Case A.1). Note that in Fig. 4.2a only the relative range variations from 300 km are shown. These plots clearly demonstrate the unstable behavior of the relative motions in the sense

of linearly increasing displacements with time. As can be seen in Figures 4.2a through 4.2c there exists a 10 km decrease in the relative range, ±1 m/s oscillations in the range-rate, and fluctuations in the relative acceleration magnitude which range from -0.002 to 0.001 m/s^2.

Table 4.3

Initial Orbital Elements of the Lead Satellite
Used for the Case A.1

Inertial Rectangular Orbital Elements			Keplerian Orbital Elements		
X (m)	=	6531262.314	a (m)	=	R_e + 160000.0
Y (m)	=	0.0	e	=	0.0
Z (m)	=	299921.040	i (deg)	=	90.0
$\dot{X}$ (m/s)	=	-358.174	ω (deg)	=	0.0
$\dot{Y}$ (m/s)	=	0.0	Ω (deg)	=	0.0
$\dot{Z}$ (m/s)	=	7799.815	M (deg)	=	2.629

Figure 4.2a

Relative Motions Characteristics for 1-Day Arc Length
with Arbitrary Initial Orbital Elements
Gravity Model: GEM-10B

Case A.1

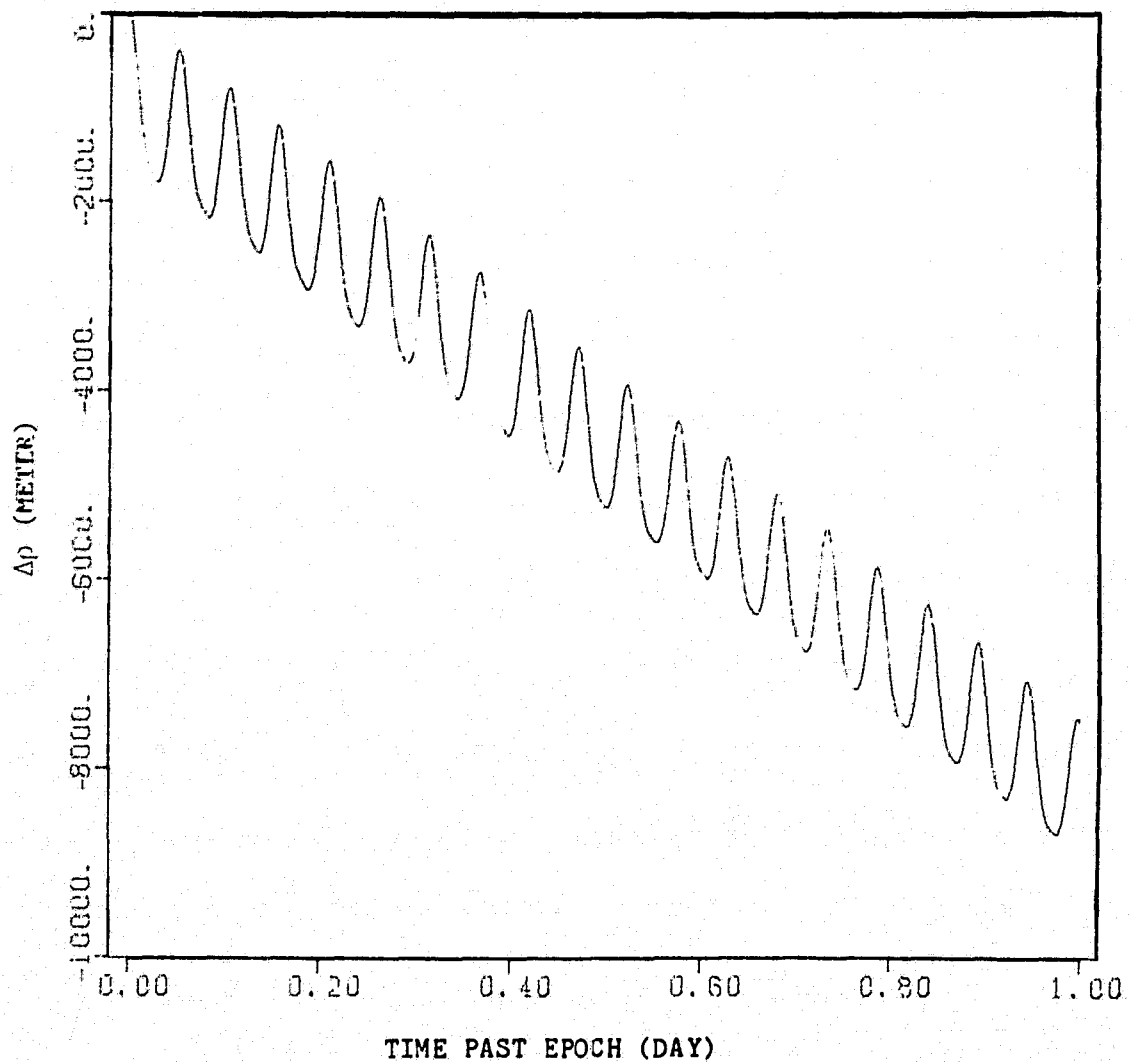Relative Range Variations from 300 km ($\Delta\rho$) vs. Time

TIME PAST EPOCH (DAY)

Figure 4.2b

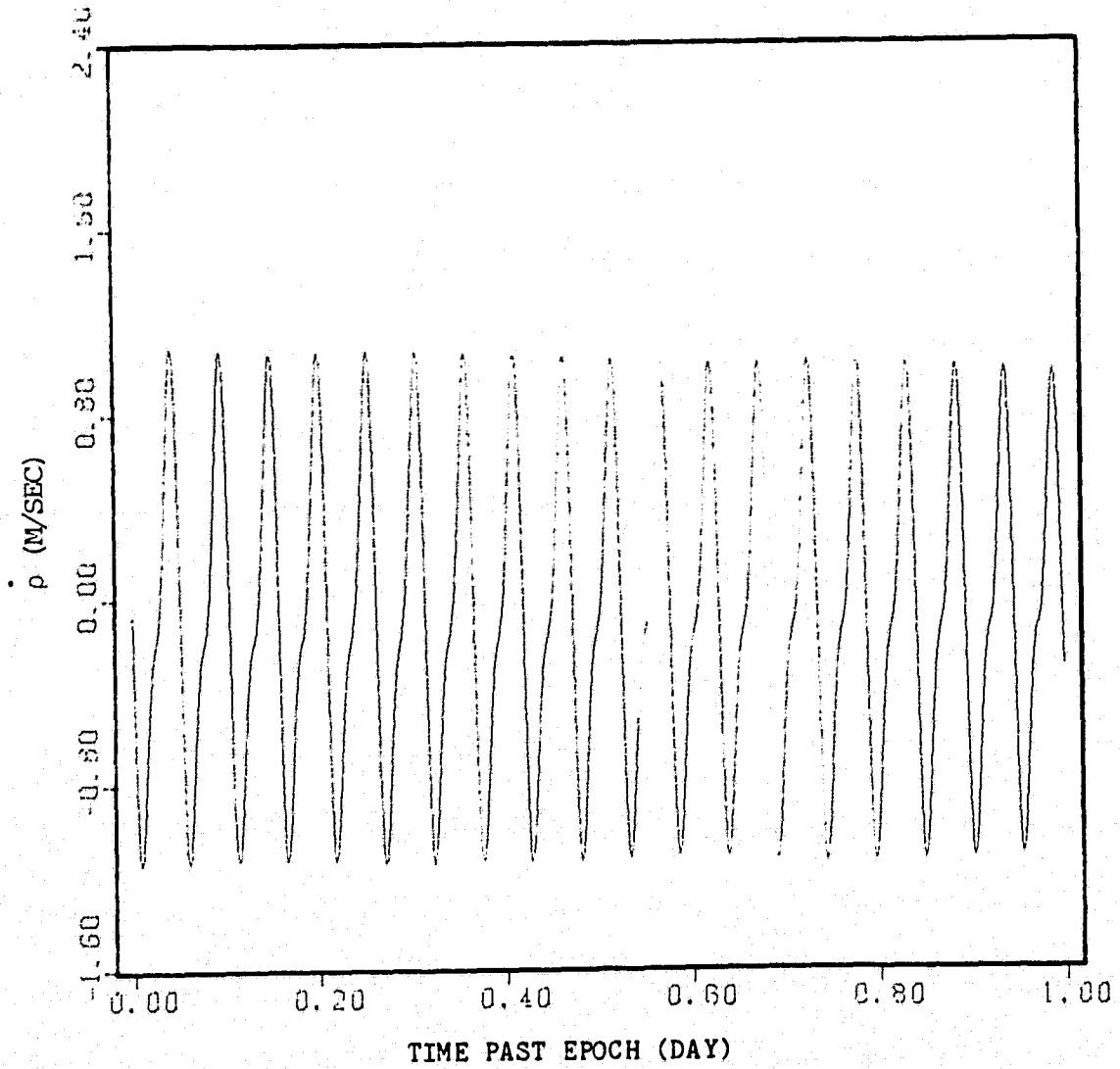Case A.1 (Continued)

Relative Range-Rate ($\dot{\rho}$) vs. Time

TIME PAST EPOCH (DAY)

Figure 4.2c

Case A.1 (Continued)

Relative Acceleration Magnitude ($\ddot{\rho}$) vs. Time

TIME PAST EPOCH (DAY)
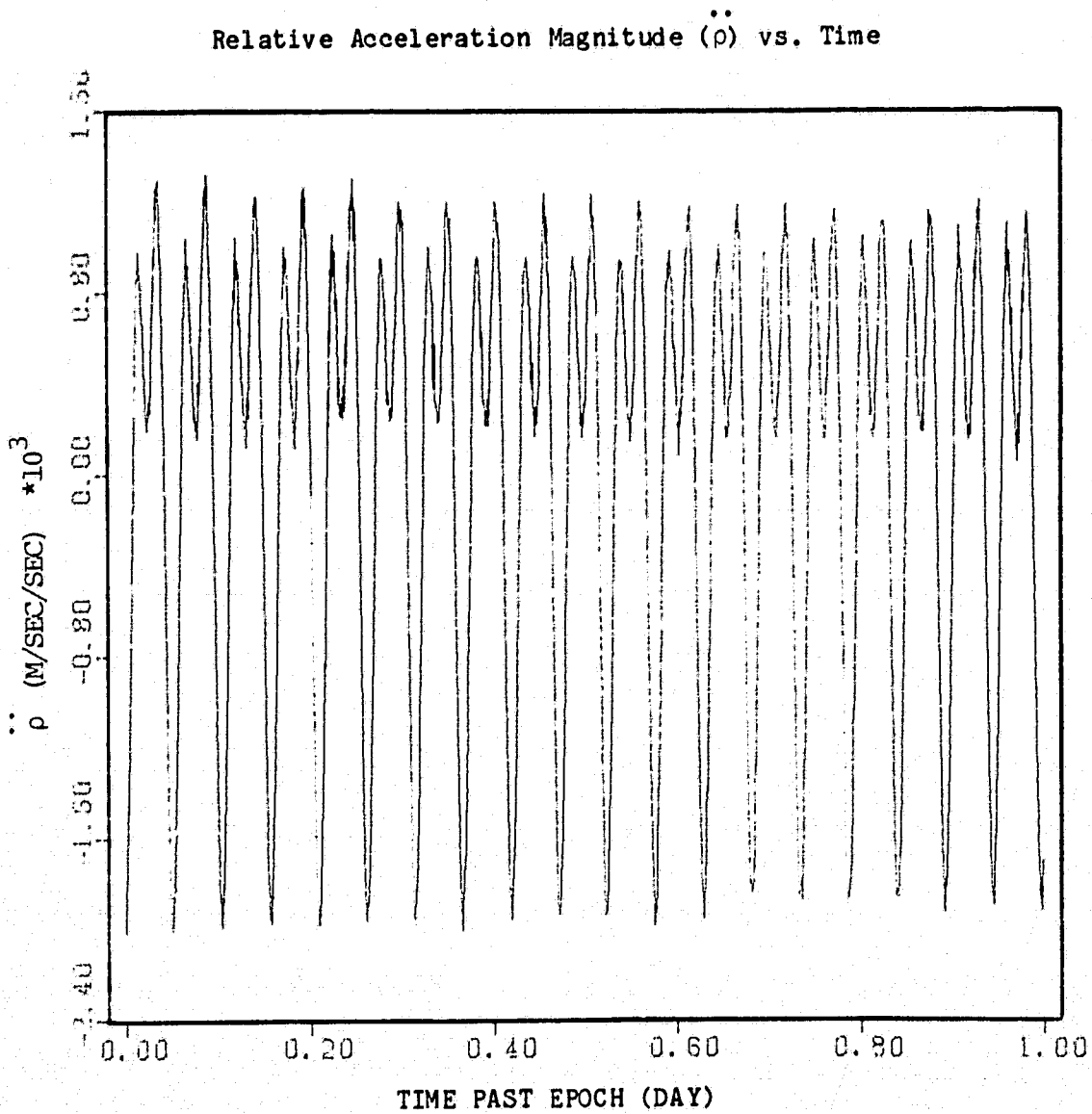
The apparent periodic oscillations in the simulations can be explained as follows. The initially selected circular orbits change to elliptical orbits due to the perturbations of the gravity field, but assuming that the satellites follow each other in the same orbit, the lead satellite starts to slow down continuously after passing through perigee at a higher rate than the trailing satellite. Consequently, the separation distance decreases until the apogee location where it reaches the minimum value. However, an opposite behavior occurs after they pass the apogee location where the lead satellite starts speeding up faster than the trailing satellite, hence resulting an increase in the separation distance until the next perigee location where the maximum separation occurs. Thus, it can be concluded that during each 90 minute revolution of the satellites the separation distance goes through a cycle with a maximum and a minimum value corresponding to the perigee and apogee locations, respectively.

Despite the large magnitude of the periodic oscillations, it is the secular change in the separation distance which essentially influences the stability of the system. The existing secular trend (Fig. 4.2a) is produced due to the presence of time dependent nonlinear terms which would appear in a series expansion of the relative motion between the two satellites. The effects of such terms can be eliminated by selecting initial orbital elements which tend to set the non-zero coefficients of the nonlinear terms to very small values or even ideally to zero. The selection of such initial orbital elements is accomplished by utilizing the optimization method which was developed in Chapter 3.

The procedure for this action is as follows.

The initial guess for the orbital elements of the lead satellite required for the Newton-Raphson iteration method are chosen to be the same as those used for the previous simulations (Case A.1). Then, following the steps of the estimation algorithm presented in Section 3.3, several iterations are performed. The resulting initial state of the lead satellite at each iteration are summarized in Table 4.4, and the converged solution is given in Table 4.5. It should be noted that since the satellites were originally set in the inertial XZ orbital plane, the corrections made to the components of the position and velocity of the lead satellite are mostly in the Y-direction. And, if the initial orbital elements had been chosen in the YZ plane, the corrections should have been made largely in the X-direction, which was validated by other experiments.

The significance of the resulting initial orbital elements is clearly reflected in the simulations which are generated again for a 1-day arc length as shown in Figures 4.3a through 4.3c (Case A.2). These simulations, compared with the simulations of Case A.1, show that the secular trend in the relative range has completely been removed, and that a remarkable reduction in the amplitude of the oscillations has also been achieved, where now only ±60 meters variations are present in the relative range simulation (Fig. 4.3a).

Table 4.4

Results of the Iteration Process to Obtain the Appropriate
Initial Orbital Elements of the Lead Satellite for 1-Day
Arc Length with the Use of the GEM-10B Gravity Model

Iter. No.	X (m)	Y (m)	Z (m)	$\dot{X}$ (m/s)	$\dot{Y}$ (m/s)	$\dot{Z}$ (m/s)
0	6531262.314	0.000	299921.040	-358.174	0.000	7799.815
1	6531244.565	-26134.483	300101.156	-358.839	10.763	7799.772
2	6531251.981	-10383.628	300209.453	-358.962	6.452	7799.763
3	6531253.126	2051.539	300214.241	-358.966	6.582	7799.759
4	6531251.485	-631.542	299977.100	-358.687	21.843	7799.762
5	6531252.199	1154.880	299967.175	-358.674	16.729	7799.760
6	6531252.237	1778.375	299960.775	-358.667	16.091	7799.760
7	6531252.238	1800.673	299959.994	-358.666	16.100	7799.760
8	6531252.238	1800.544	299960.014	-358.666	16.100	7799.761

Table 4.5

Appropriate Initial Orbital Elements of the Lead Satellite
Obtained for 1-Day Arc Length with the Use of the GEM-10B Gravity Model

Inertial Rectangular Orbital Elements		Keplerian Orbital Elements	
X (m) =	6531252.238	a (m) =	R_e + 159959.107
Y (m) =	1800.544	e =	0.569137 E-04
Z (m) =	299960.014	i (deg) =	89.881
$\dot{X}$ (m/s) =	-358.666	ω (deg) =	97.700
$\dot{Y}$ (m/s) =	16.100	Ω (deg) =	0.010
$\dot{Z}$ (m/s) =	7799.761	M (deg) =	264.936

Figure 4.3a

Relative Motions Characteristics for 1-Day Arc Length
with Appropriate Initial Orbital Elements
Gravity Model: GEM-10B

Case A.2

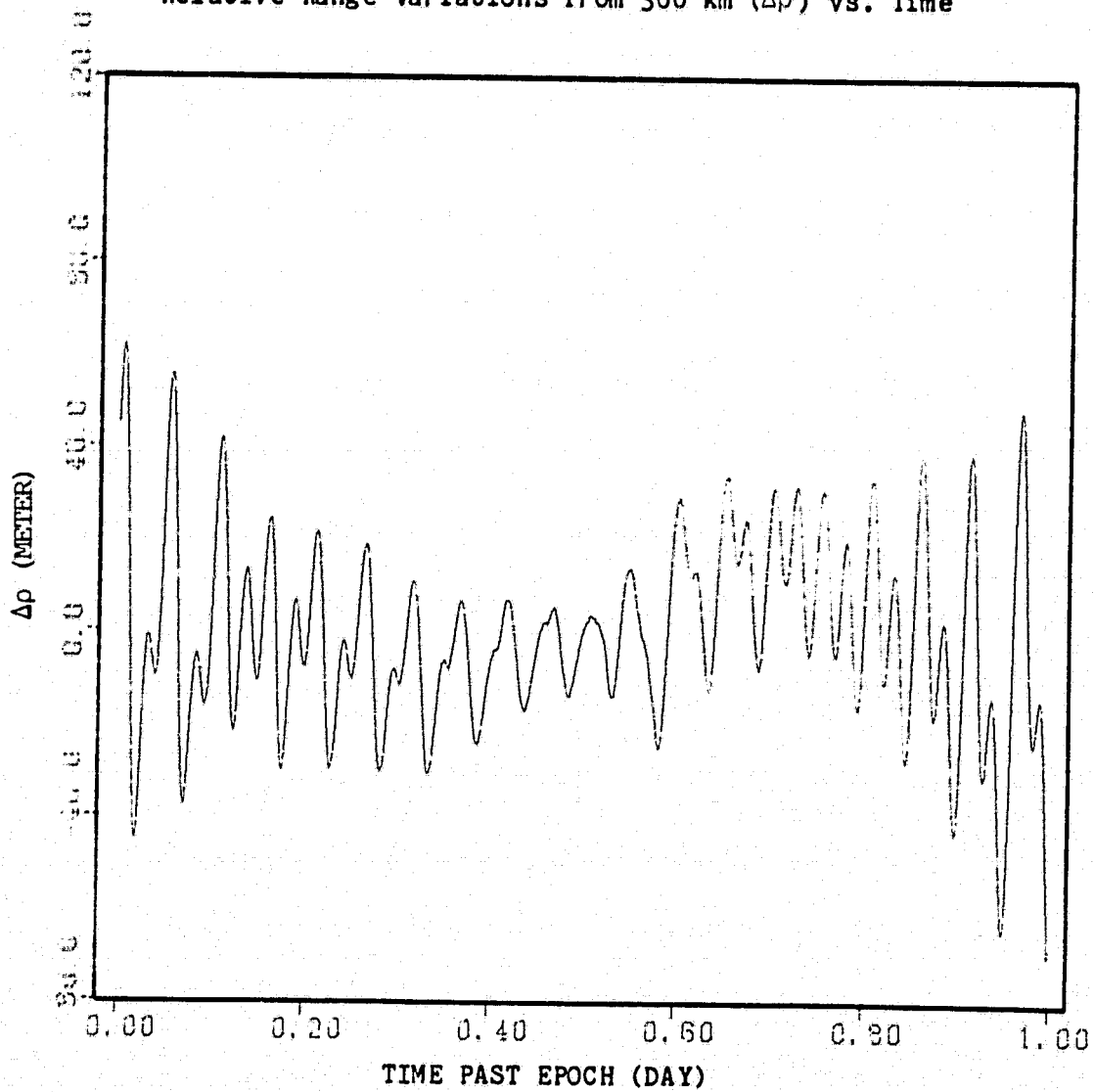**Relative Range Variations from 300 km ($\Delta\rho$) vs. Time**
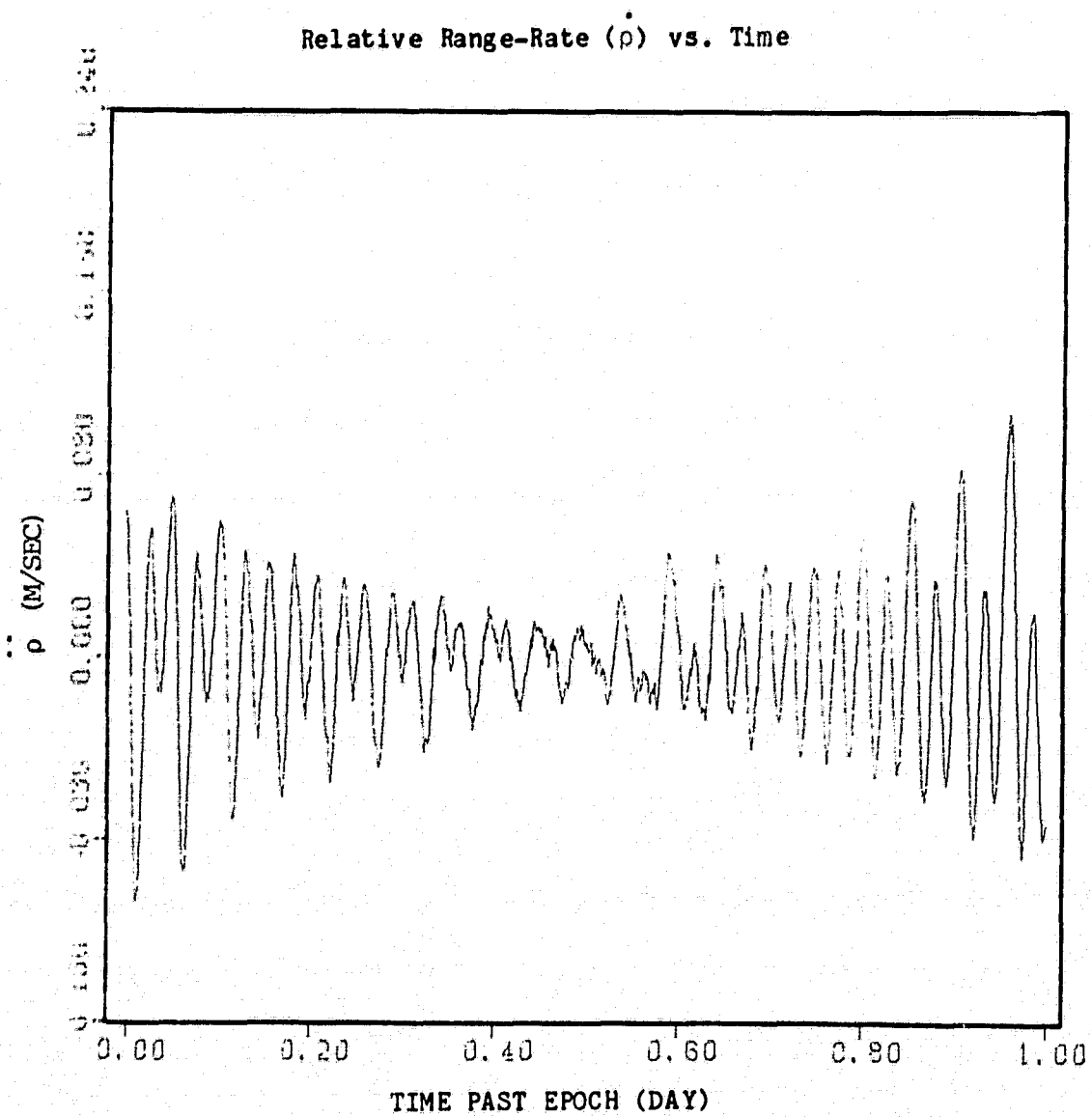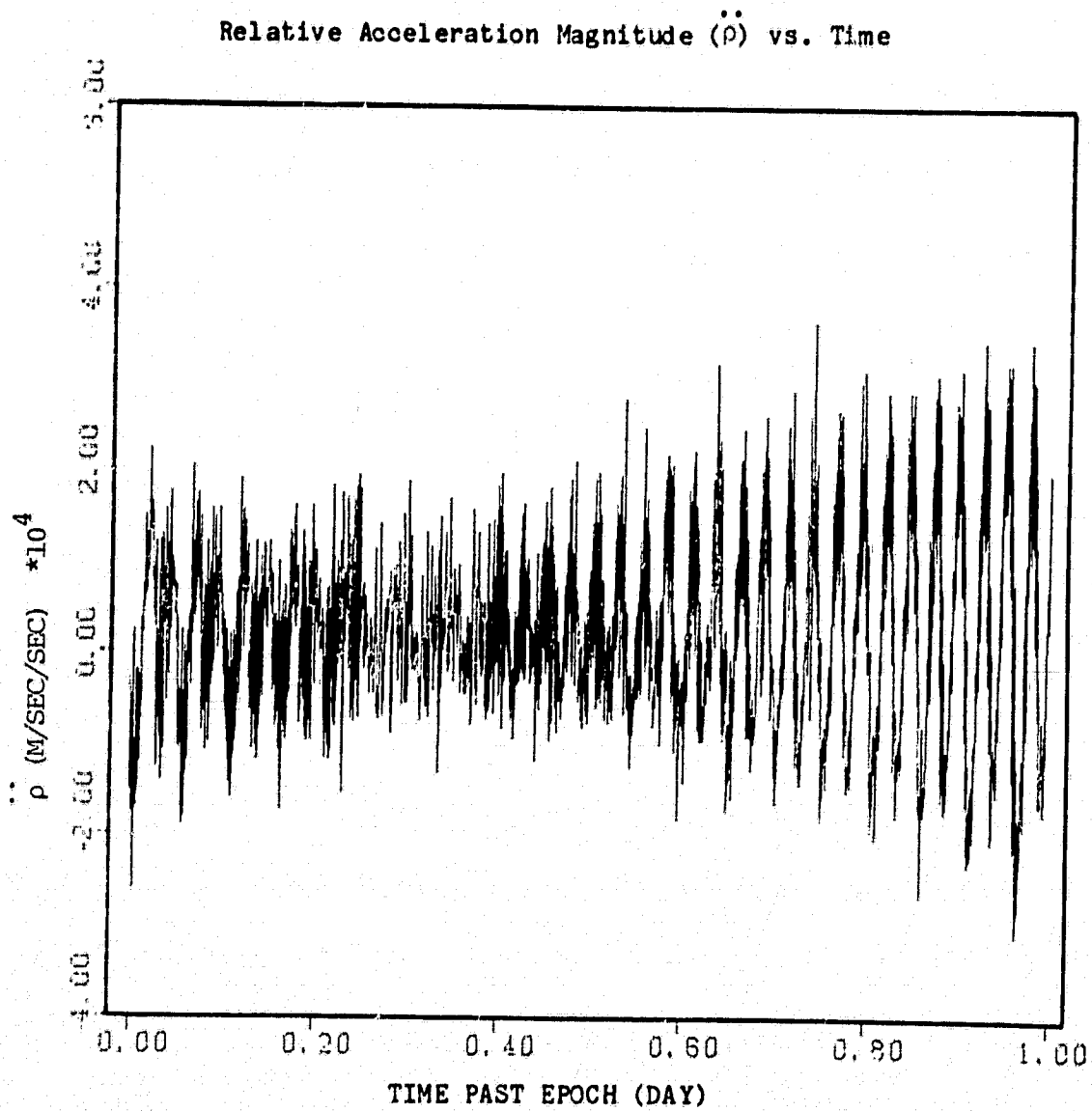
Figure 4.3b

Case A.2 (Continued)

Relative Range-Rate ($\dot{\rho}$) vs. Time

Figure 4.3c

Case A.2 (Continued)

Relative Acceleration Magnitude ($\ddot{\rho}$) vs. Time

TIME PAST EPOCH (DAY)

In order to demonstrate the effects of the GEM-10B gravity field model for a longer time period, the obtained initial orbital elements for Case A.2 are used to generate the simulations for 3-day arc length which are shown in Figures 4.4a, b, c (Case A.3). Obviously, the stable behavior is only present for the first day of the simulations and after that a divergent type behavior is developed where a 400 m decrease in the relative range is produced (Fig. 4.4c). However, using the same procedure as followed for Case A.2, an appropriate initial state is obtained which provides stable behavior throughout the 3-day arc length. The initial state used for the iteration process of this case (Case A.4) is chosen to be the one obtained for the 1-day arc length, and the resulting initial orbital elements are given in Table 4.6. The generated simulations for this case are shown in Figures 4.5a, b, c. Note again the considerable reduction in the level of fluctuations which are achieved by the use of appropriate initial orbital elements.

Table 4.6

Appropriate Initial Orbital Elements of the Lead Satellite
Obtained for 3-Day Arc Length with the Use of the GEM-10B Gravity Model

Inertial Rectangular Orbital Elements		Keplerian Orbital Elements	
X (m) =	6531248.413	a (m) =	R_e + 159958.499
Y (m) =	3635.284	e =	0.540248 E-04
Z (m) =	299944.245	i (deg) =	89.884
$\dot{X}$ (m/s) =	-358.630	ω (deg) =	97.454
$\dot{Y}$ (m/s) =	15.602	Ω (deg) =	0.027
$\dot{Z}$ (m/s) =	7799.768	M (deg) =	265.181

Figure 4.4a

Relative Motions Characteristics for 3-Day Arc Length
with the Initial Orbital Elements of Case A.2
Gravity Model: GEM-10B
Case A.3

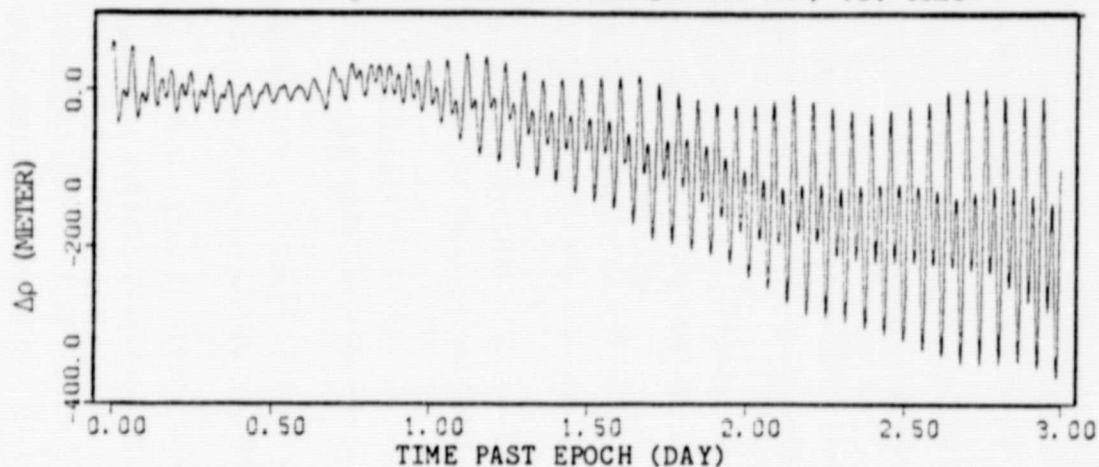Relative Range Variations from 300 km (Δρ) vs. Time

Figure 4.5a

Relative Motions Characteristics for 3-Day Arc Length
with Appropriate Initial Orbital Elements
Gravity Model: GEM-10B
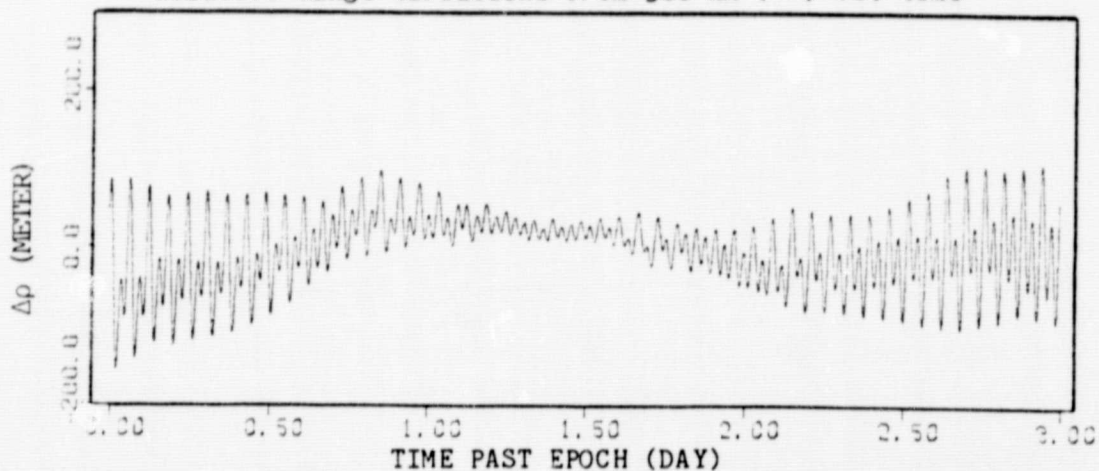Case A.4

Relative Range Variations from 300 km (Δρ) vs. Time
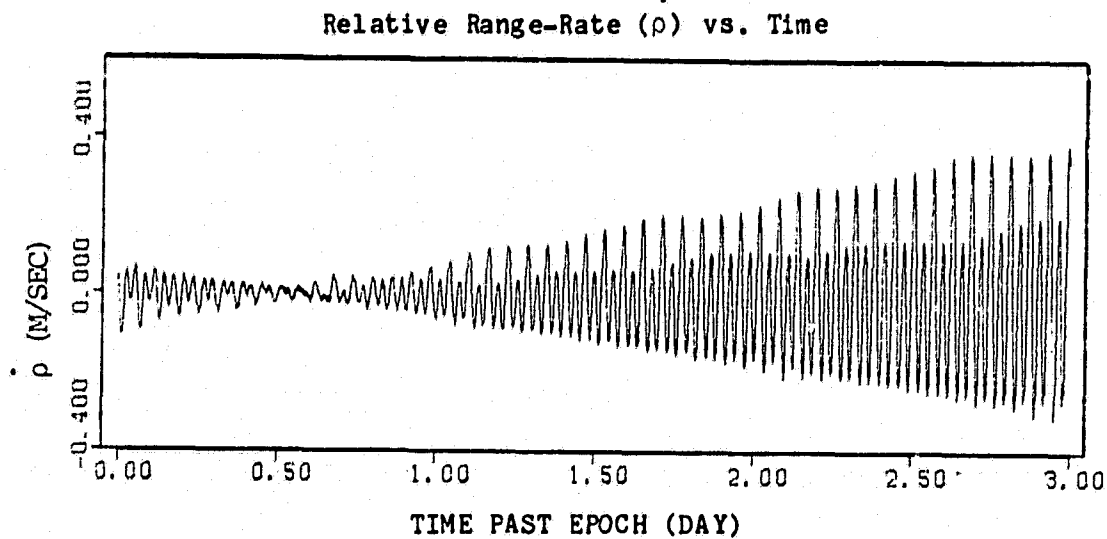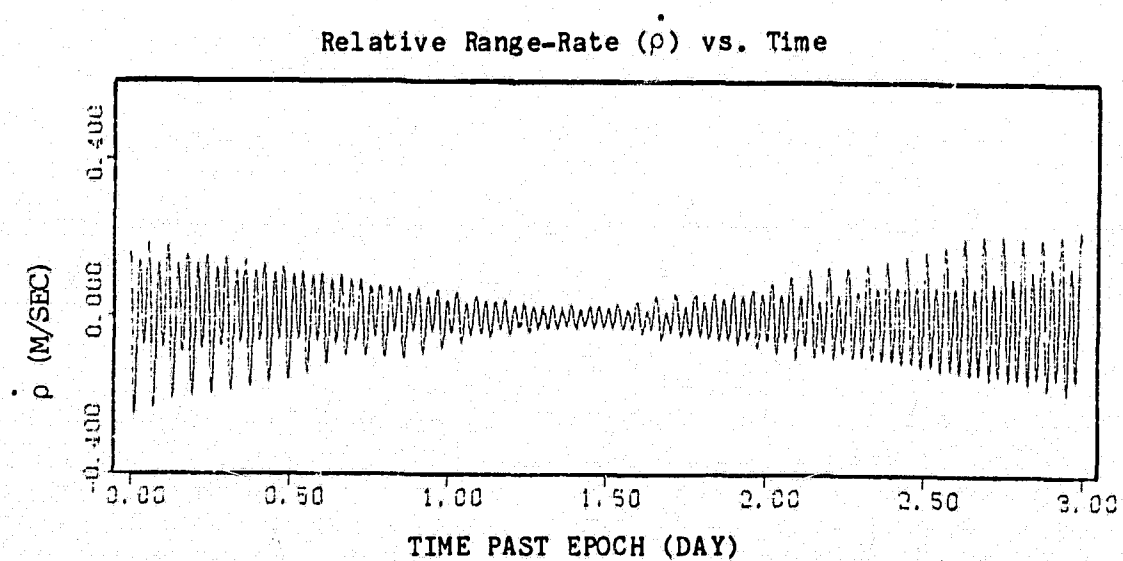
Figure 4.4b

Case A.3 (Continued)

Relative Range-Rate ($\dot{\rho}$) vs. Time

TIME PAST EPOCH (DAY)

Figure 4.5b

Case A.4 (Continued)

Relative Range-Rate ($\dot{\rho}$) vs. Time

TIME PAST EPOCH (DAY)

Figure 4.4c

Case A.3 (Continued)

Relative Acceleration Magnitude ($\ddot{\rho}$) vs. Time

TIME PAST EPOCH (DAY)
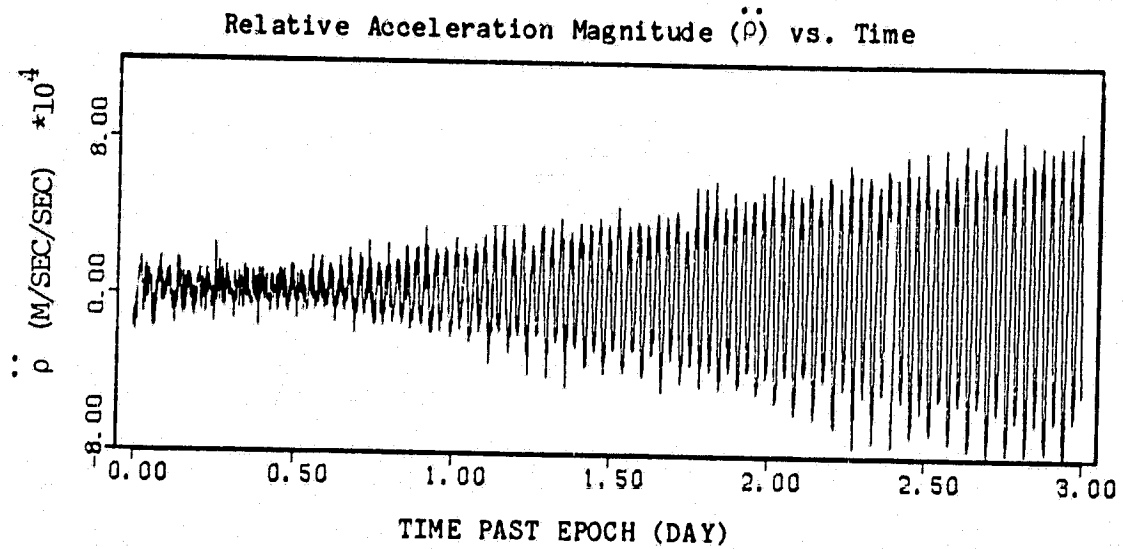
Figure 4.5c

Case A.4 (Continued)

Relative Acceleration Magnitude ($\ddot{\rho}$) vs. Time

TIME PAST EPOCH (DAY)
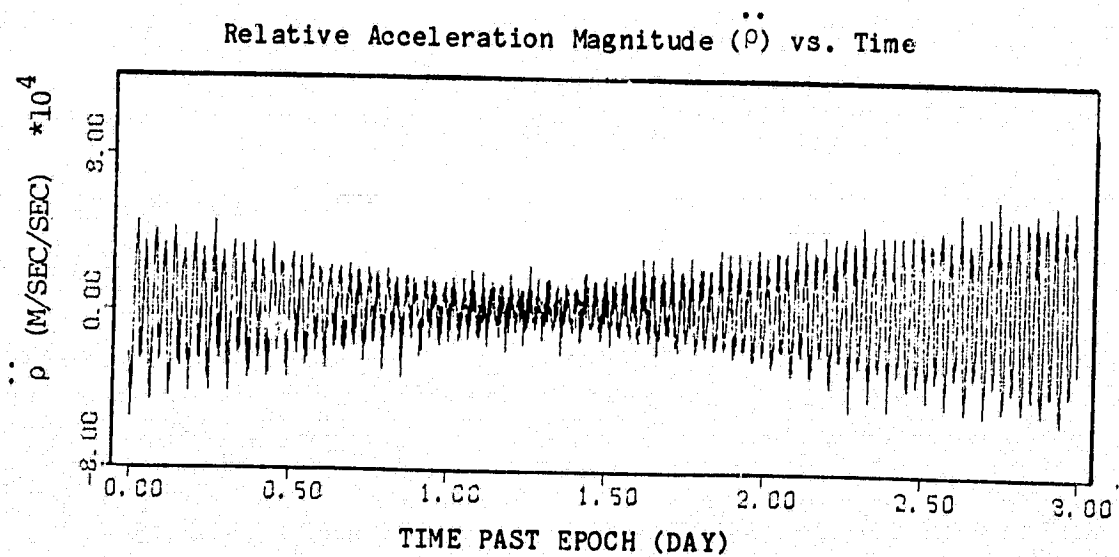
The prediction of the relative motions characteristics was carried out for 6-day and 12-day arc lengths. Following identical procedure as was done for Case A.4, appropriate sets of initial orbital elements were obtained for 6-day and 12-day arc lengths which are given in Tables 4.7 and 4.8, respectively. The generated simulations for 6-day arc length using the obtained initial orbital elements for 3-day and 6-day arc lengths are plotted as shown in Figures 4.6a, b, c (Case A.5) and Figures 4.7a, b, c (Case A.6) respectively. Also, the generated simulations for the 12-day arc length using the obtained initial orbital elements for 6-day and 12-day arc lengths are shown in Figures 4.8a, b, c (Case A.7) and Figures 4.9a, b, c (Case A.8), respectively. Note the successive reduction in the levels of variations in the simulations for equal arc lengths. For example, comparing the simulations obtained for Case A.8 with Case A.7, a 50% reduction in the order of magnitude of the oscillations are achieved.

The initial components of the position and velocity of the lead satellite obtained for various arc lengths are tabulated in Tables 4.9a and 4.9b respectively. Note the consistent differences between each set of initial orbital elements. For longer time intervals the obtained initial states have a larger components for the position and a smaller components for the velocity in the inertial Y-direction. These initial orbital elements obtained for the lead satellite compared with the ones specified for the trailing satellite (Table 4.2) clearly indicate that the satellites move on very close orbits but not the same one.

Table 4.7

Appropriate Initial Orbital Elements of the Lead Satellite
Obtained for 6-Day Arc Length with the Use of the GEM-10B Gravity Model

Inertial Rectangular Orbital Elements			Keplerian Orbital Elements		
X (m)	=	6531233.103	a (m)	=	R_e + 159958.528
Y (m)	=	6495.894	e	=	0.485553 E-04
Z (m)	=	300078.439	i (deg)	=	89.901
$\dot{X}$ (m/s)	=	-358.753	ω (deg)	=	96.741
$\dot{Y}$ (m/s)	=	13.198	Ω (deg)	=	0.052
$\dot{Z}$ (m/s)	=	7799.775	M (deg)	=	265.895

Table 4.8

Appropriate Initial Orbital Elements of the Lead Satellite
Obtained for 12-Day Arc Length with the Use of the GEM-10B Gravity Model

Inertial Rectangular Orbital Elements			Keplerian Orbital Elements		
X (m)	=	6531193.906	a (m)	=	R_e + 159958.501
Y (m)	=	7170.572	e	=	0.401601 E-04
Z (m)	=	300266.230	i (deg)	=	89.943
$\dot{X}$ (m/s)	=	-358.912	ω (deg)	=	91.094
$\dot{Y}$ (m/s)	=	7.382	Ω (deg)	=	0.060
$\dot{Z}$ (m/s)	=	7799.811	M (deg)	=	271.543

Figure 4.6a

Relative Motions Characteristics for 6-Day Arc Length
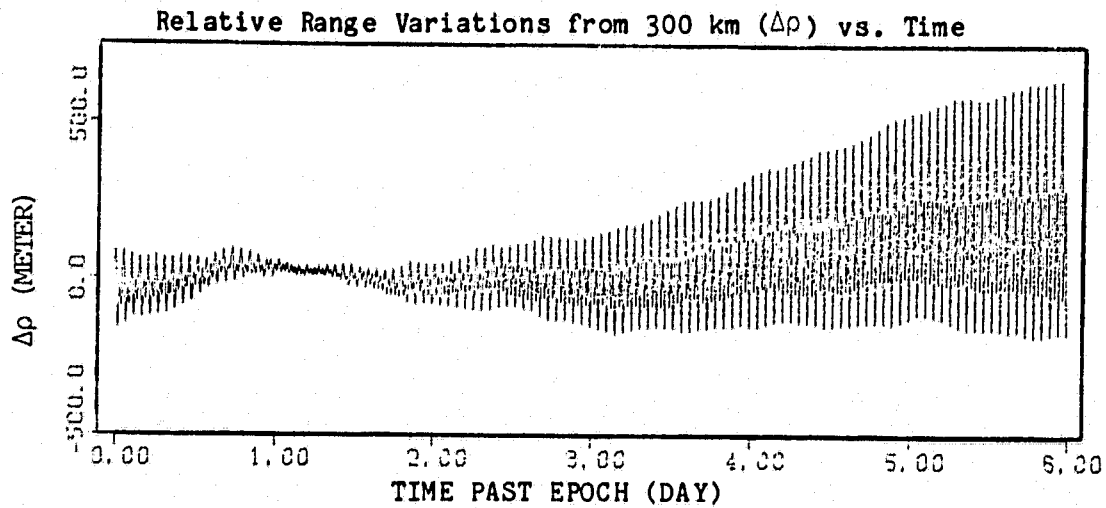with the Initial Orbital Elements of Case A.4
Gravity Model: GEM-10B
Case A.5

Relative Range Variations from 300 km ($\Delta\rho$) vs. Time

Figure 4.7a

Relative Motions Characteristics for 6-Day Arc Length
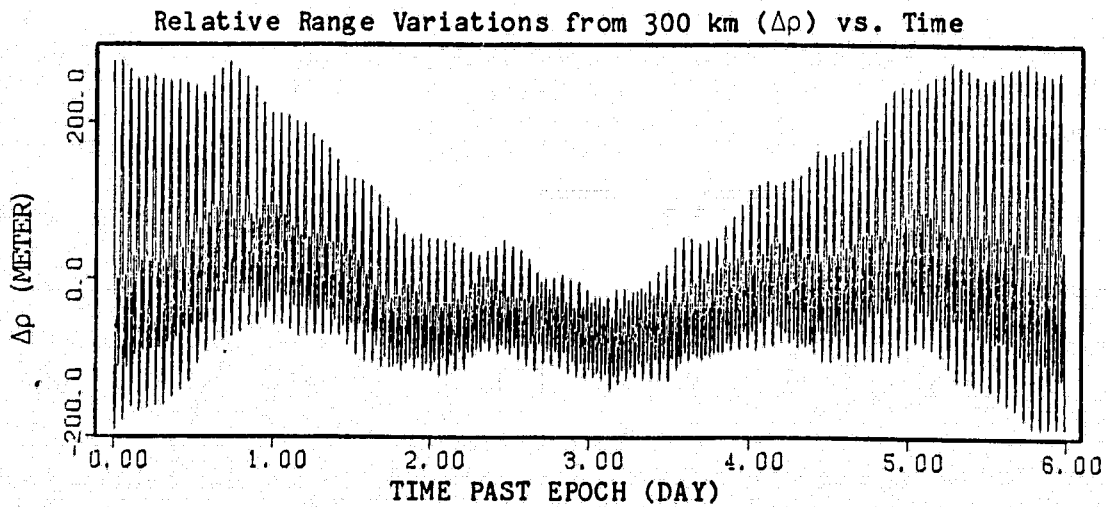with Appropriate Initial Orbital Elements
Gravity Model: GEM-10B
Case A.6

Relative Range Variations from 300 km ($\Delta\rho$) vs. Time
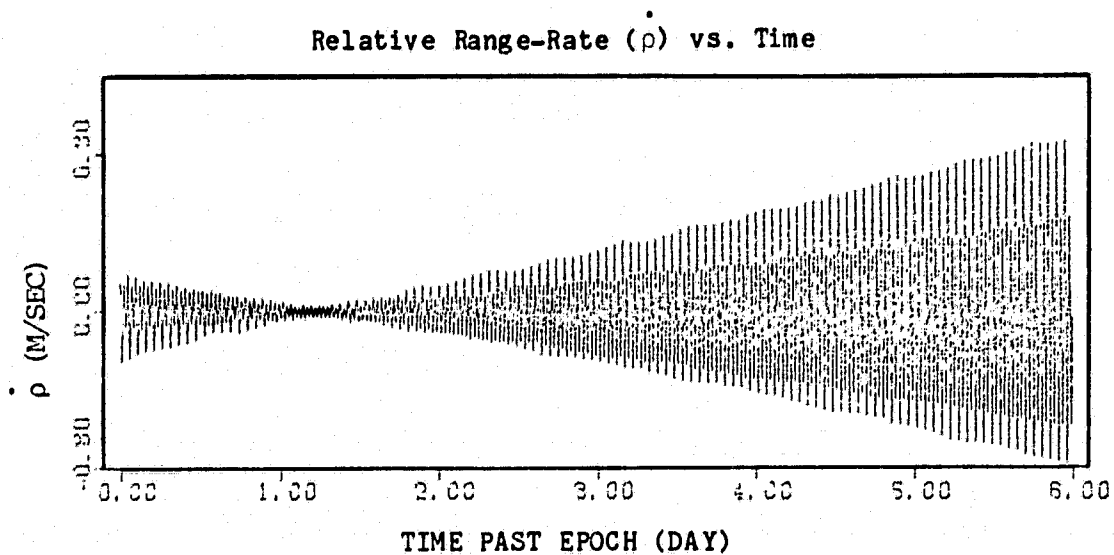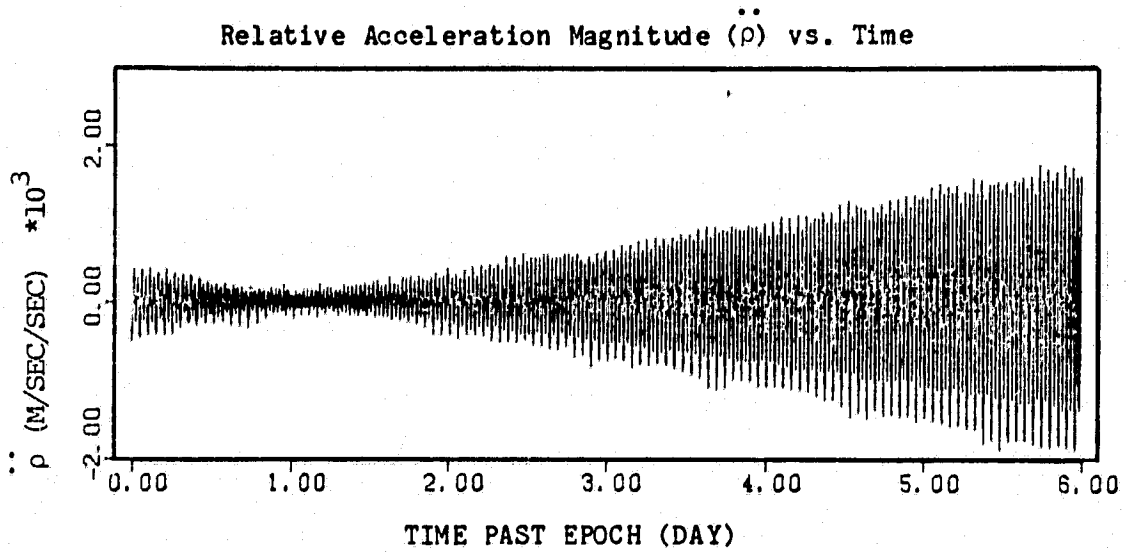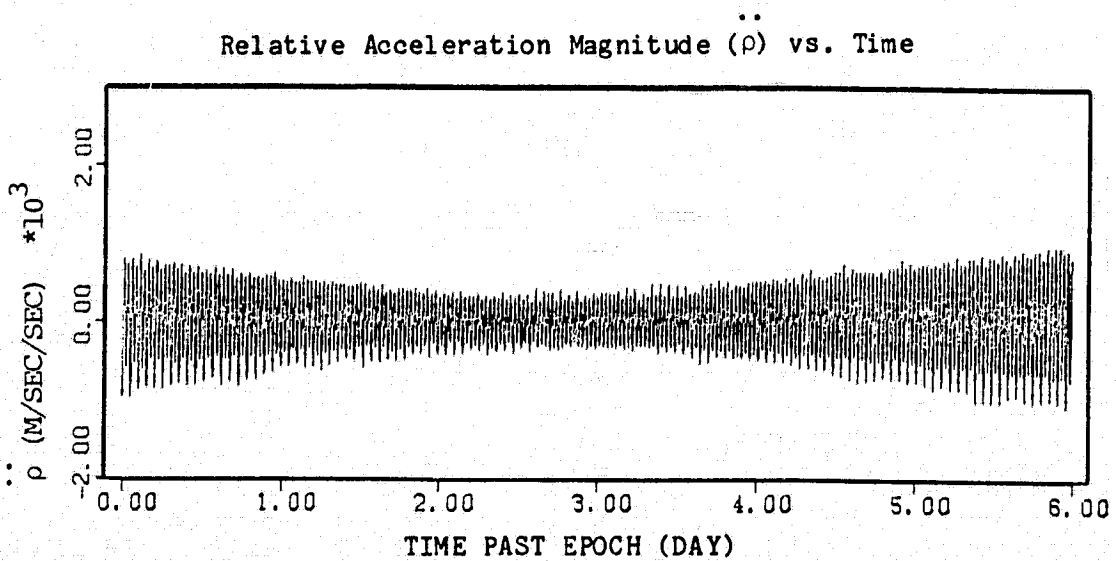
Figure 4.6b

Case A.5 (Continued)

Relative Range-Rate ($\dot{\rho}$) vs. Time

TIME PAST EPOCH (DAY)

Figure 4.7b

Case A.6 (Continued)

Relative Range-Rate ($\dot{\rho}$) vs. Time

TIME PAST EPOCH (DAY)
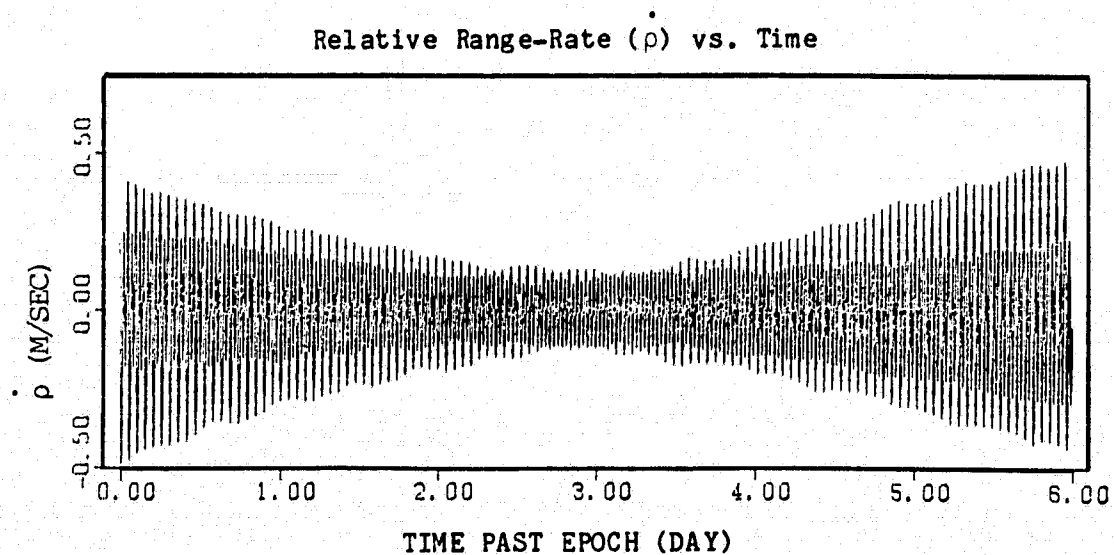
Figure 4.6c

Case A.5 (Continued)

Relative Acceleration Magnitude ($\ddot{\rho}$) vs. Time

Figure 4.7c

Case A.6 (Continued)

Relative Acceleration Magnitude ($\ddot{\rho}$) vs. Time

Figure 4.8a

Relative Motions Characteristics for 12-Day Arc Length
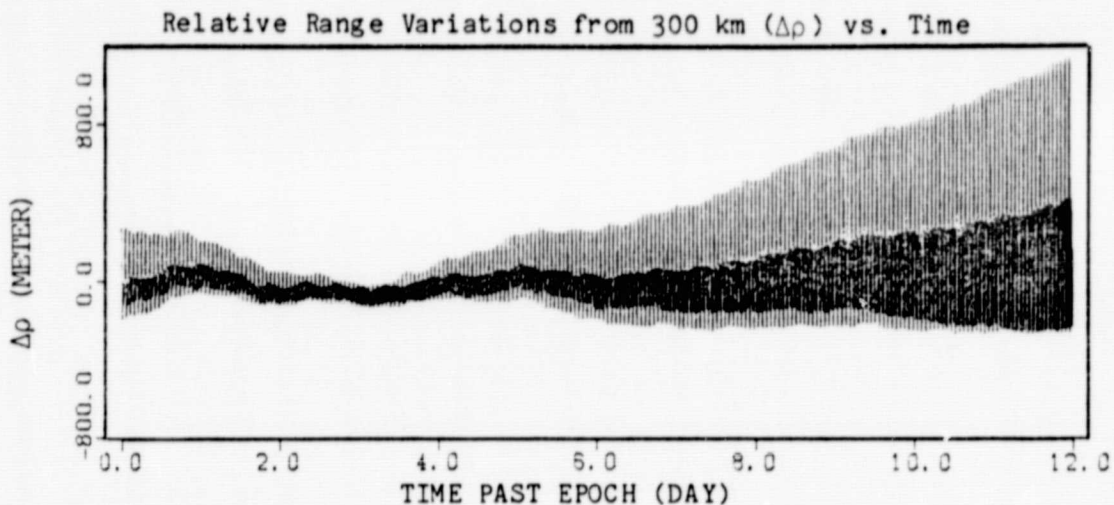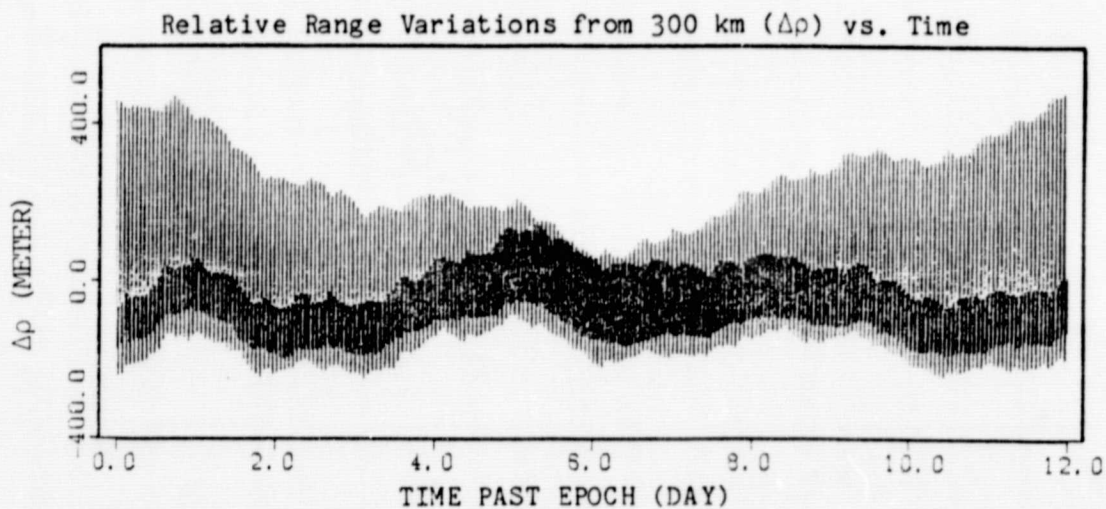with the Initial Orbital Elements of Case A.6
Gravity Model: GEM-10B
Case A.7

Relative Range Variations from 300 km (Δρ) vs. Time

Figure 4.9a

Relative Motions Characteristics for 12-Day Arc Length
with Appropriate Initial Orbital Elements
Gravity Model: GEM-10B
Case A.8

Relative Range Variations from 300 km (Δρ) vs. Time

Figure 4.8b

Case A.7 (Continued)

Relative Range-Rate ($\dot{\rho}$) vs. Time
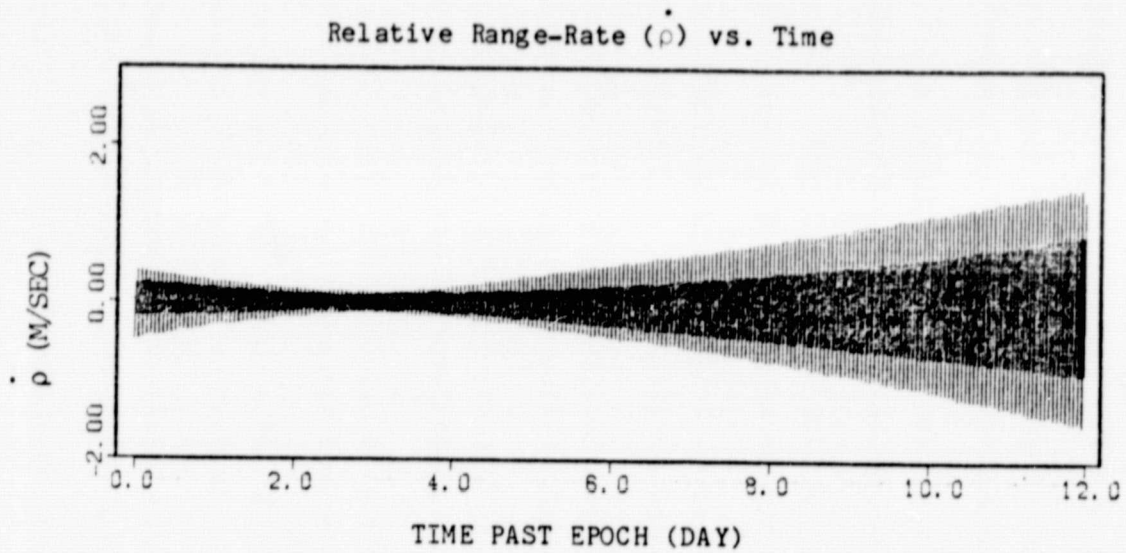
Figure 4.9b

Case A.8 (Continued)

Relative Range-Rate ($\dot{\rho}$) vs. Time
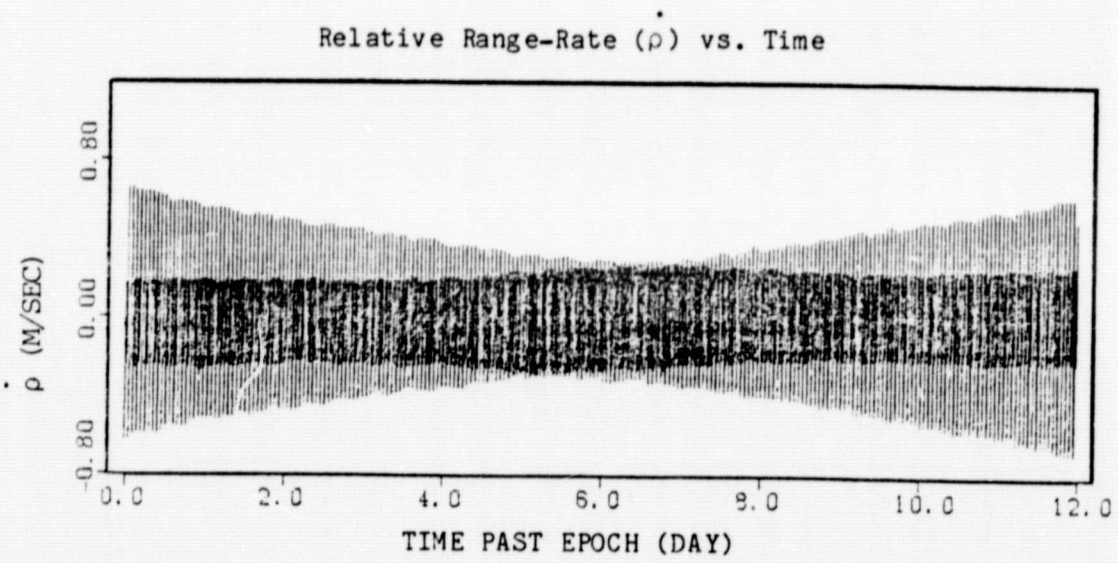
Figure 4.8c

Case A.7 (Continued)

Relative Acceleration Magnitude ($\ddot{\rho}$) vs. Time

Figure 4.9c

Case A.8 (Continued)

Relative Acceleration Magnitude ($\ddot{\rho}$) vs. Time
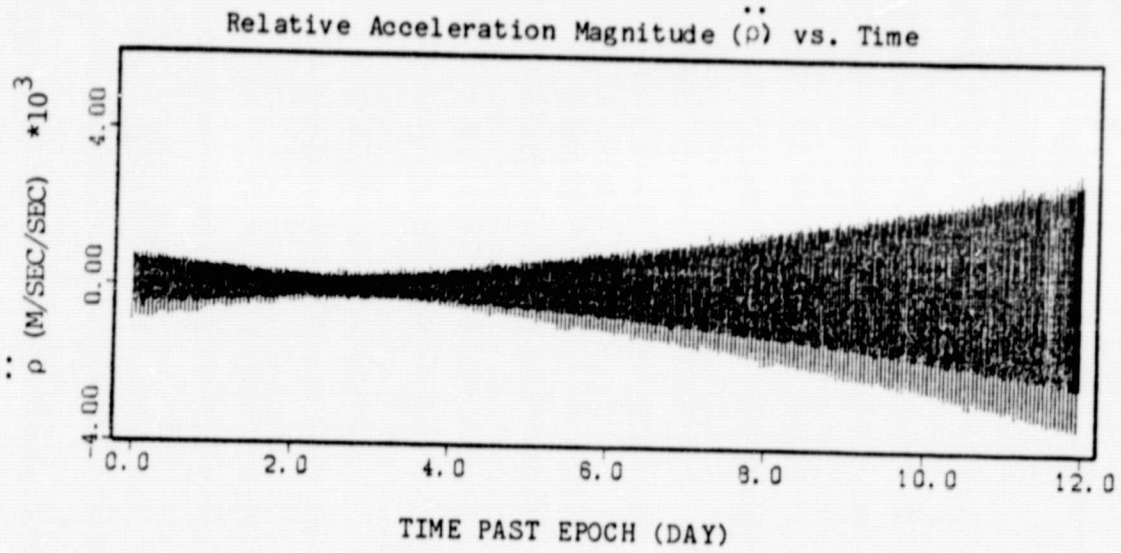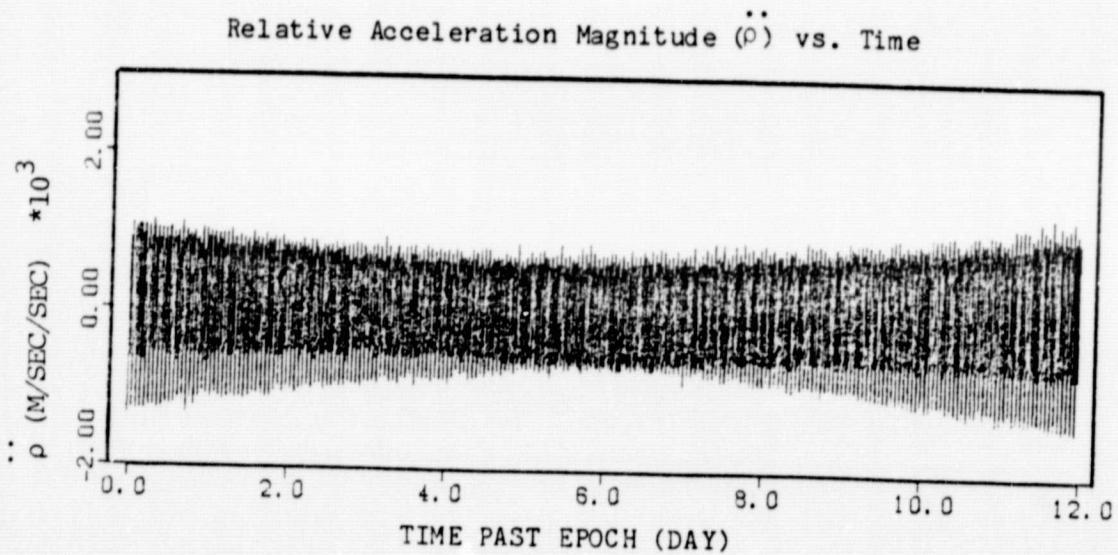
Table 4.9a

Appropriate Inertial Position Components of the Initial State
of the Lead Satellite Obtained for Various Time Intervals
with the use of the GEM-10B Gravity Model

Arc Length	X (m)	Y (m)	Z (m)	r (m)
1-Day	6531252.238	1800.544	299960.014	R_e + 159991.971
3-Day	6531248.413	3635.284	299944.245	R_e + 159988.189
6-Day	6531233.103	6495.894	300078.439	R_e + 159981.270
12-Day	6531193.906	7170.572	300266.230	R_e + 159951.441

Table 4.9b

Appropriate Inertial Velocity Components of the Initial State
of the Lead Satellite Obtained for Various Time Intervals
with the use of the GEM-10B Gravity Model

Arc Length	$\dot{X}$ (m/s)	$\dot{Y}$ (m/s)	$\dot{Z}$ (m/s)	v (m/s)
1-Day	-358.666	16.100	7799.761	7808.020
3-Day	-358.630	15.602	7799.768	7808.024
6-Day	-358.753	13.198	7799.775	7808.032
12-Day	-358.912	7.382	7799.811	7808.068

4.4 Effect of Error in the Second Degree Zonal Harmonic Coefficient

The second degree zonal harmonic coefficient of the geopotential expansion, given by Eq. (2.1), is denoted by J_2. The motion of a satellite is dominantly perturbed by the effect of the J_2 which represents the earth's oblateness. Therefore, in this section the J_2 coefficient of the GEM-10B gravity model is purposely altered by a slight amount in order to demonstrate the produced effects in the relative motion simulations due to this change. The simulations procedures are as follows.

The normalized J_2 coefficient of the GEM-10B gravity model has the value of -0.4841655 E-03 and was increased by 1.0 E-08 for the simulation to produce the effect of an error in the coefficient. The initial orbital elements of the lead satellite, which were obtained for Case A.2, were used to simulate the relative motions. The difference between the obtained simulations for this case (Case B.1) and the ones obtained for Case A.2 are shown in Figures 4.10a through 4.10c.

The same initial orbital elements were used to obtain an appropriate set of initial orbital elements for the lead satellite which remove the small secular trend in the separation distance which is apparent in Fig. 4.10a. This was accomplished by applying the same optimization method as before. The obtained initial state of the lead satellite for this case (Case B.2) is given in Table 4.10. Once again, the simulations obtained for this case are differenced with the simulations of Case A.2 and the results are plotted as shown in Figures 4.11a

through 4.11c. These simulations compared with the simulations of Case B.1 indicate a well-behaved periodic oscillations which represent the significance of the obtained initial orbital elements.

Table 4.10

Appropriate Initial Orbital Elements of the Lead Satellite
Obtained for 1-Day Arc Length with the use of
Gravity Model: GEM-10B $+ \Delta J_2$

Inertial Rectangular Orbital Elements			Keplerian Orbital Elements		
X (m)	=	6531252.184	a (m)	=	R_e + 159959.107
Y (m)	=	1813.933	e	=	0.568937 E-04
Z (m)	=	299960.613	i (deg)	=	89.881
$\dot{X}$ (m/s)	=	-358.667	ω (deg)	=	97.698
$\dot{Y}$ (m/s)	=	16.080	Ω (deg)	=	0.010
$\dot{Z}$ (m/s)	=	7799.761	M (deg)	=	264.938

Figure 4.10a

Relative Motions Perturbations Due to $\Delta J_2 = 10^{-8}$
of the GEM-10B Model for 1-Day Arc Length with
the Initial Orbital Elements of Case A.2
Case B.1

Relative Range Perturbations $(\delta\rho)$ vs. Time
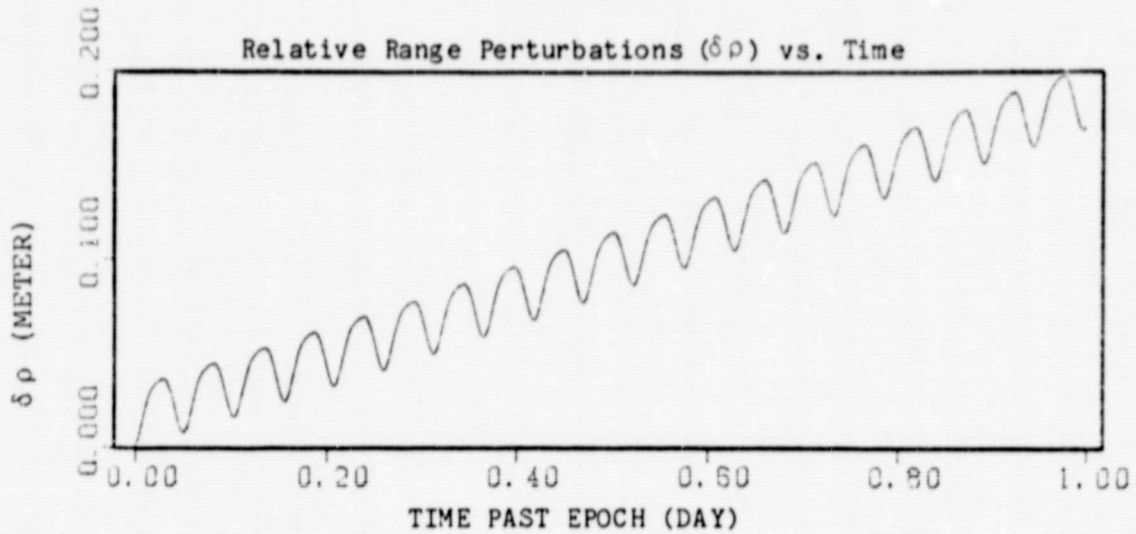

TIME PAST EPOCH (DAY)

Figure 4.11a

Relative Motions Perturbations Due to $\Delta J_2 = 10^{-8}$
of the GEM-10B Model for 1-Day Arc Length
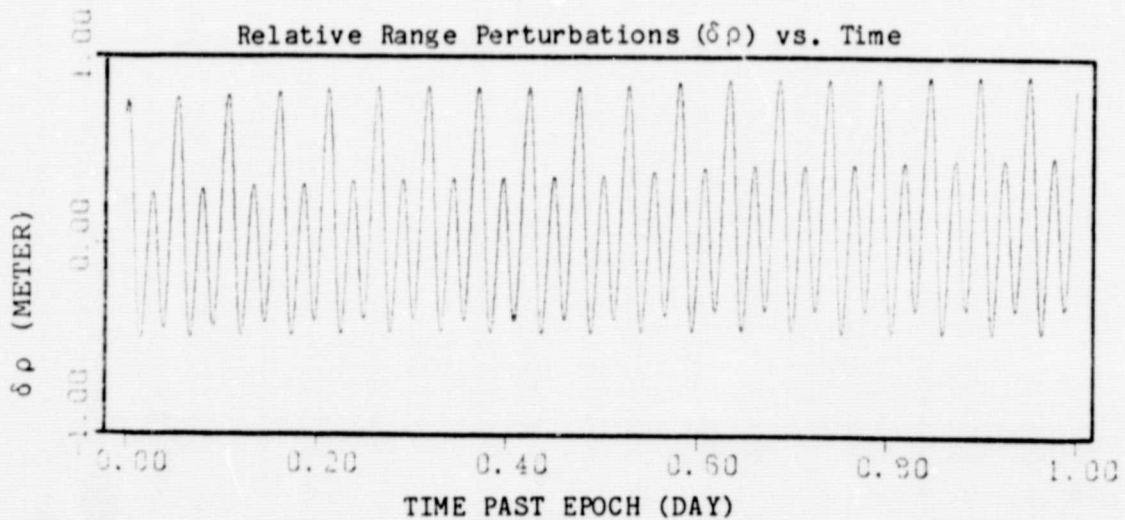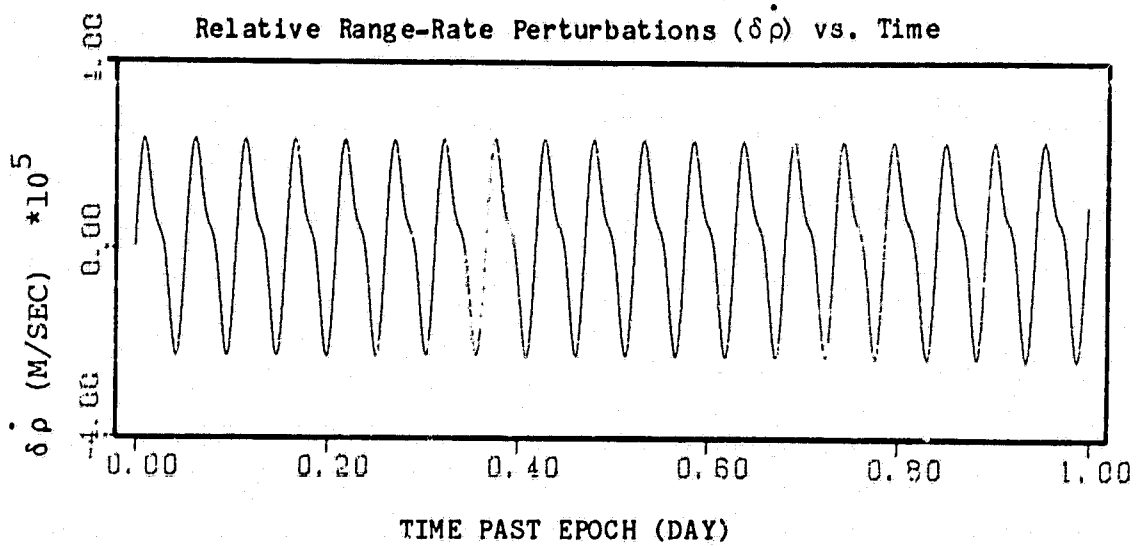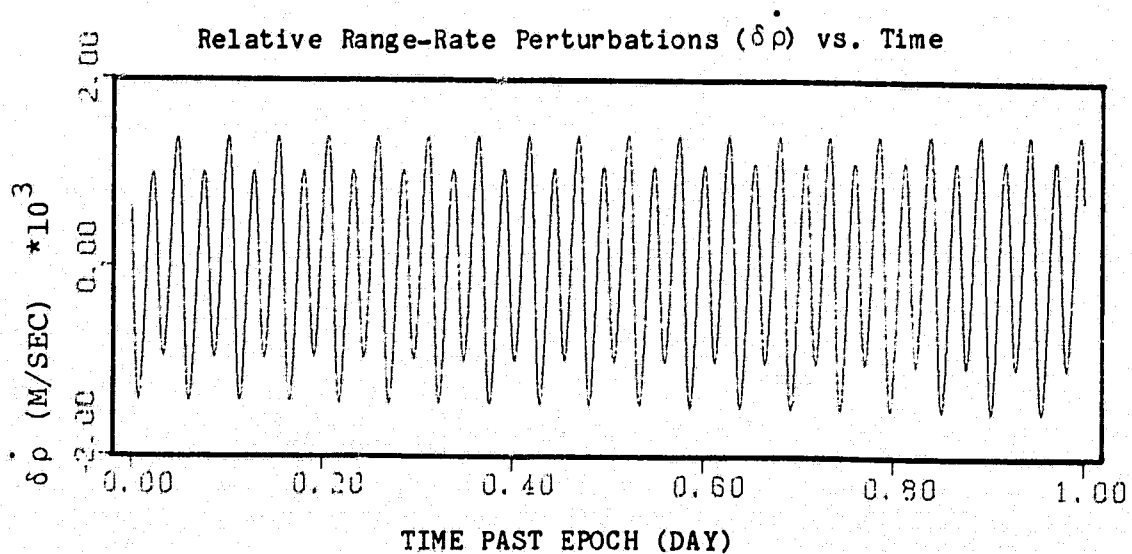with Appropriate Initial Orbital Elements
Case B.2

Relative Range Perturbations $(\delta\rho)$ vs. Time

TIME PAST EPOCH (DAY)

Figure 4.10b

Case B.1 (Continued)

Relative Range-Rate Perturbations ($\delta\dot{\rho}$) vs. Time

TIME PAST EPOCH (DAY)

Figure 4.11b

Case B.2 (Continued)

Relative Range-Rate Perturbations ($\delta\dot{\rho}$) vs. Time

TIME PAST EPOCH (DAY)

4.5 Effects of the Gravity Model Error

So far in this chapter it has been assumed that the GEM-10B gravity model represents the most accurate model of the earth's gravitational field and all of the relative motions simulations were obtained with the use of GEM-10B model. In addition, a special case was also treated in Section 3.4 where a set of simulations were provided in order to demonstrate the effects of a possible error in the J_2 coefficient of the GEM-10B model (Cases B.1-2). However, in this section the effects of a full gravity model error in the relative motions are demonstrated in which the GEM-9 model which has harmonics complete to degree and order 22 is assumed to represent the "true" gravity model of the earth.

The initial orbital elements of the lead satellite which were obtained for Case A.2 (given in Table 4.5) are used to simulate the relative motions under the influence of the GEM-9 gravity model. The resulting simulations are plotted as shown in Figures 4.12a through 4.12c (Case C.1) and the differences between these simulations and the ones obtained for Case A.2 are shown in Figures 4.13a through 4.13c (Case C.2). Note that because of the different energy of the GEM-9 model, the stable behavior of the relative motions in Case A.2 is completely changed to an irregularly secular behavior in which a 600 meters error in the separation distance is produced (Fig. 4.13a).

Figure 4.12a

Relative Motions Characteristics for 1-Day Arc Length
with the Initial Orbital Elements of Case A.2
Gravity Model: GEM-9
Case C.1

Relative Range Variations from 300 km ($\Delta\rho$) vs. Time
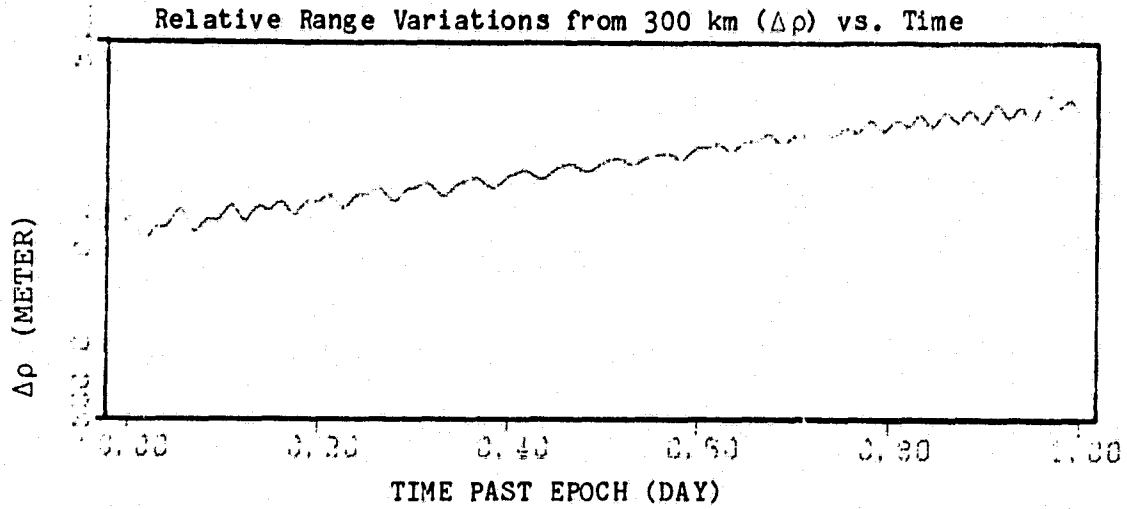

TIME PAST EPOCH (DAY)

Figure 4.13a

Relative Motions Differences between GEM-10B and GEM-9 Models
for 1-Day Arc Length with the Initial Orbital
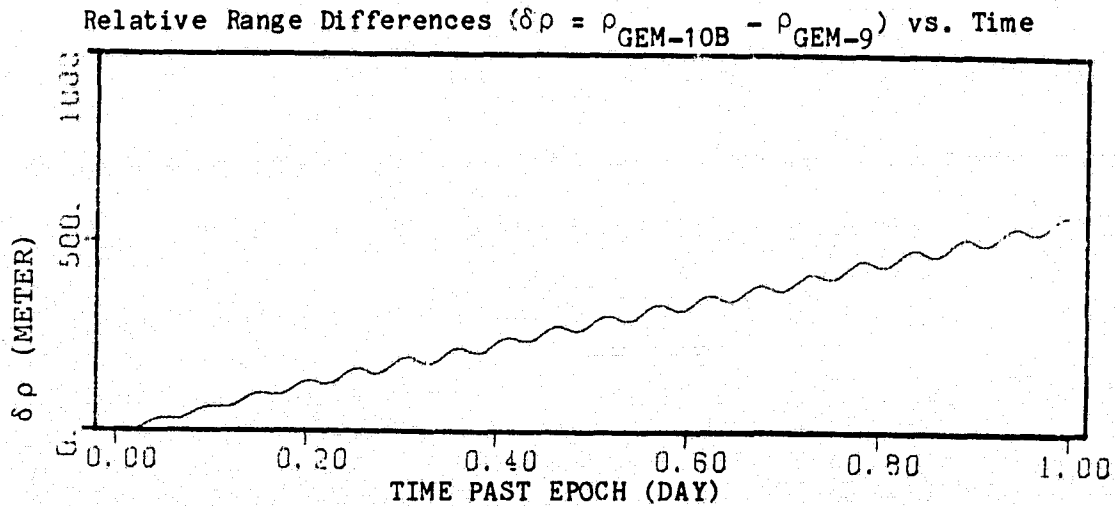Elements of Case A.2 Used for each Model
Case C.2

Relative Range Differences ($\delta\rho = \rho_{GEM-10B} - \rho_{GEM-9}$) vs. Time

TIME PAST EPOCH (DAY)

Figure 4.12b

Case C.1 (Continued)

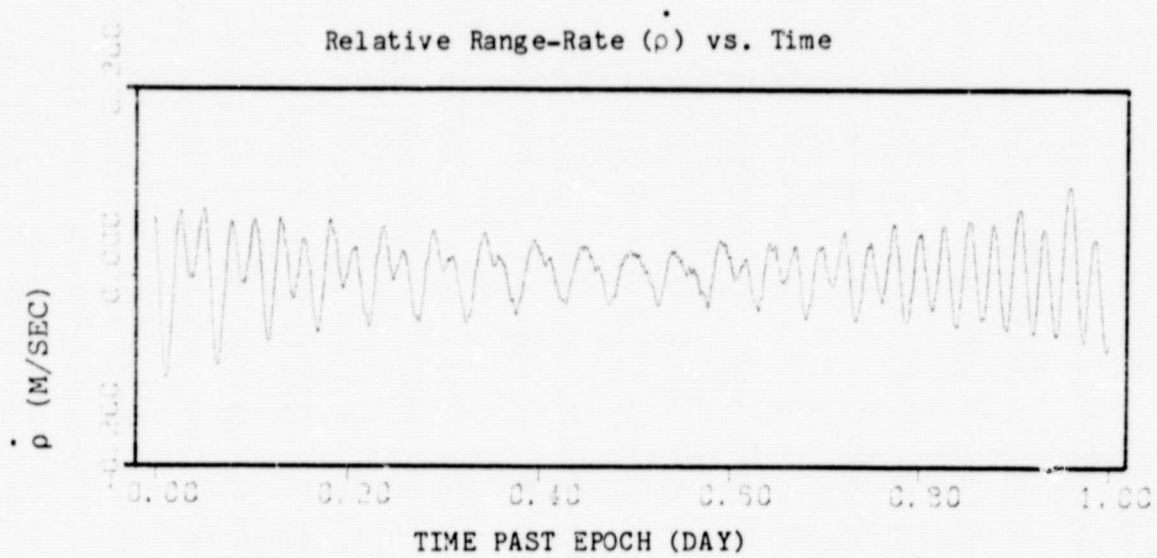### Relative Range-Rate ($\dot{\rho}$) vs. Time

TIME PAST EPOCH (DAY)

Figure 4.13b

Case C.2 (Continued)

Relative Range-Rate Differences ($\delta\dot{\rho}$) vs. Time

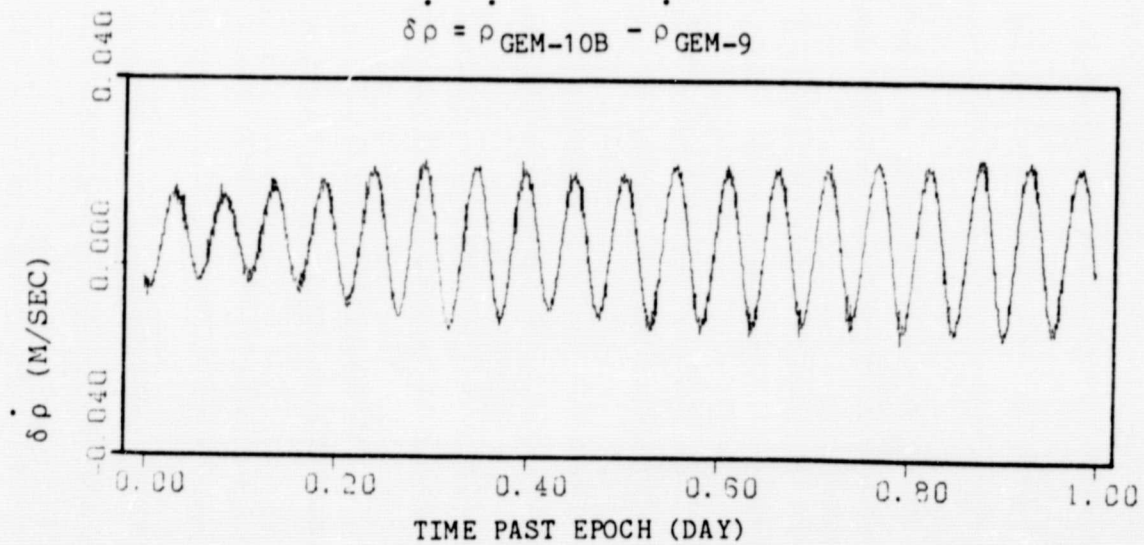$$\delta\dot{\rho} = \dot{\rho}_{GEM-10B} - \dot{\rho}_{GEM-9}$$

TIME PAST EPOCH (DAY)

Figure 4.12c

Case C.1 (Continued)

Relative Acceleration Magnitude ($\ddot{\rho}$) vs. Time
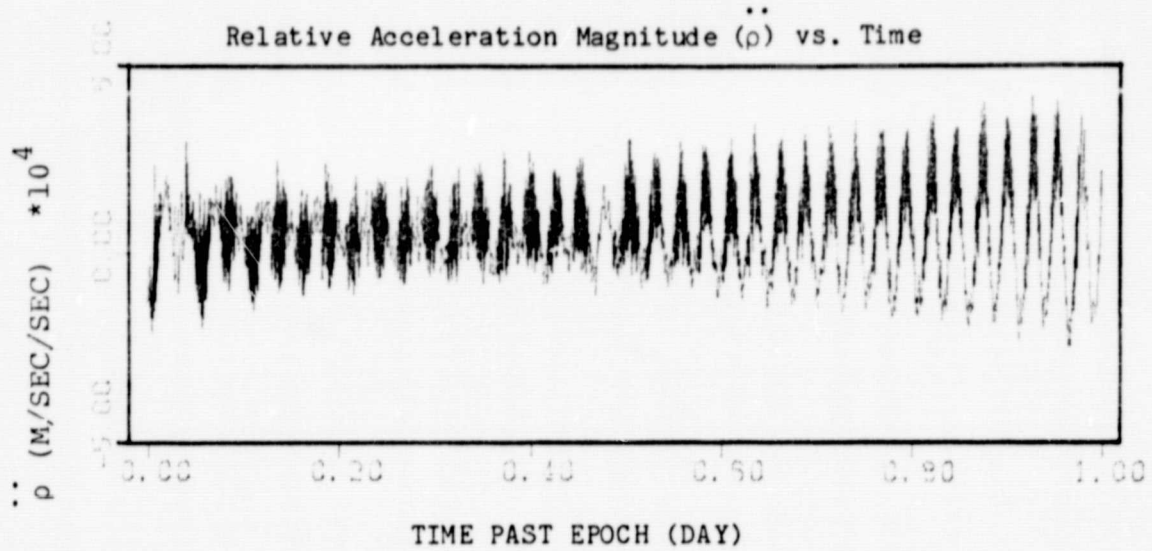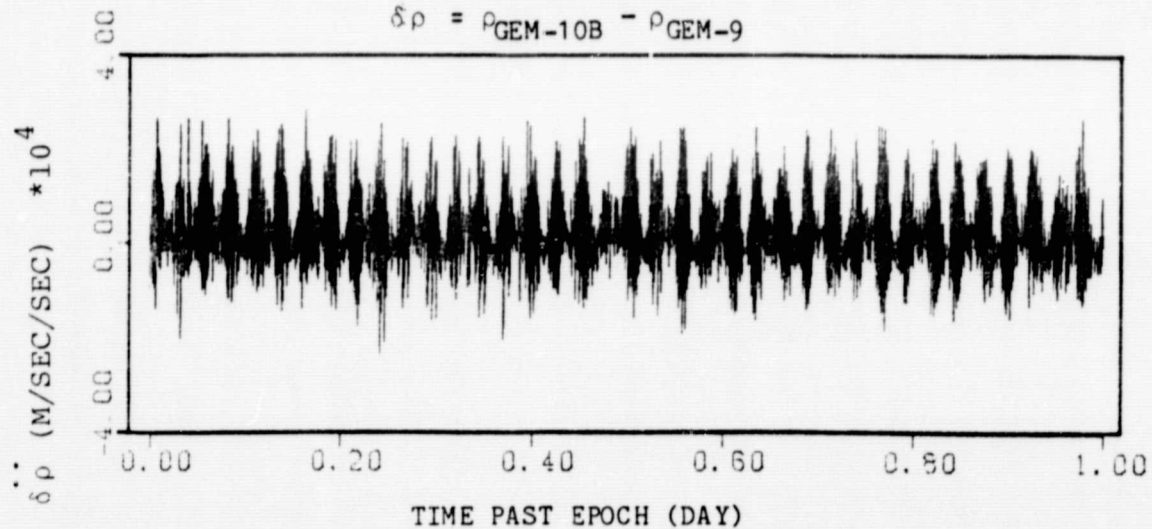
$\ddot{\rho}$ (M/SEC/SEC) $*10^4$

TIME PAST EPOCH (DAY)

Figure 4.13c

Case C.2 (Continued)

Relative Acceleration Magnitude Differences ($\delta\ddot{\rho}$) vs. Time

$$\delta\ddot{\rho} = \ddot{\rho}_{GEM-10B} - \ddot{\rho}_{GEM-9}$$

$\delta\ddot{\rho}$ (M/SEC/SEC) $*10^4$

TIME PAST EPOCH (DAY)

The same initial orbital elements are used to obtain appropri-
ate set of initial orbital elements such that the generated simulations
best fit the simulations of Case A.2 in a least squares sense. This is
accomplished by minimizing the performance index which can be expressed
as

$$P = \int_0^{1-\text{day}} \{ \rho_{\text{GEM}-10B} - \rho_{\text{GEM}-9} \}^2 \, dt$$

where $\rho_{\text{GEM}-10B}$ represents the relative range between the two satellites
computed at some instant of time with the use of GEM-9 model; whereas,
$\rho_{\text{GEM}-10B}$ represents the corresponding relative range computed at the
same instant of time with the use of GEM-10B gravity model. The pro-
cedure to minimize the above function is basically the same as that
presented in Section 3.3. Therefore, after performing several itera-
tions, the final adjusted initial orbital elements for the lead satel-
lite are obtained which are given in Table 4.11. Then, the obtained
initial orbital elements are used to generate the simulations with the
use of GEM-9 model. These simulations as well as their differences with
the simulations obtained with the use of the GEM-10B model are shown in
Figures 4.14a through 4.14c (Case C.3), and Figures 4.15a through 4.15c
(Case C.4) respectively. Note the obtained ±16 meters error in Fig.
4.15a as compared with the previously existed 600 meters error in Fig.
4.13a.

Table 4.11

Appropriate Initial Orbital Elements of the Lead Satellite
Obtained for 1-Day Arc Length with the use of
Gravity Model: GEM-9

Inertial Rectangular Orbital Elements		Keplerian Orbital Elements		
X (m) =	6531251.338	a (m) =	R_e + 159962.234	
Y (m) =	1826.607	e =	0.574876 E-04	
Z (m) =	299945.957	i (deg) =	89.881	
$\dot{X}$ (m/s) =	-358.655	ω (deg) =	96.936	
$\dot{Y}$ (m/s) =	16.081	Ω (deg) =	0.011	
$\dot{Z}$ (m/s) =	7799.765	M (deg) =	265.700	

Having obtained the appropriate initial orbital elements, the
error in the relative motions is predicted for six days. The simula-
tions for a 6-day arc length using the GEM-9 model are shown in Figures
4.16a through 4.16c (Case C.5), and their differences with the ones
obtained with the use of the GEM-10B model are shown in Figures 4.17a
through 4.17c (Case C.6). Note again the 600 meters error in the
separation distance which is produced during the additional five days of
the simulations.

Figure 4.14a

Relative Motions Characteristics for 1-Day Arc Length
with Appropriate Initial Orbital Elements
Gravity Model: GEM-9
Case C.3

Relative Range Variations from 300 km ($\Delta\rho$) vs. Time
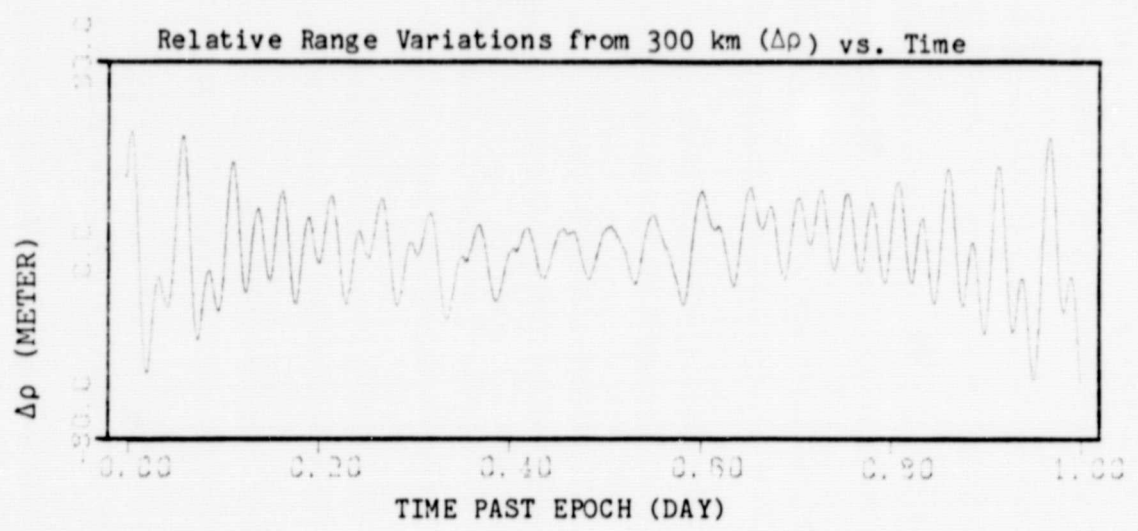

Figure 4.15a

Relative Motions Differences between GEM-10B and GEM-9 Models
for 1-Day Arc Length with Appropriate Initial
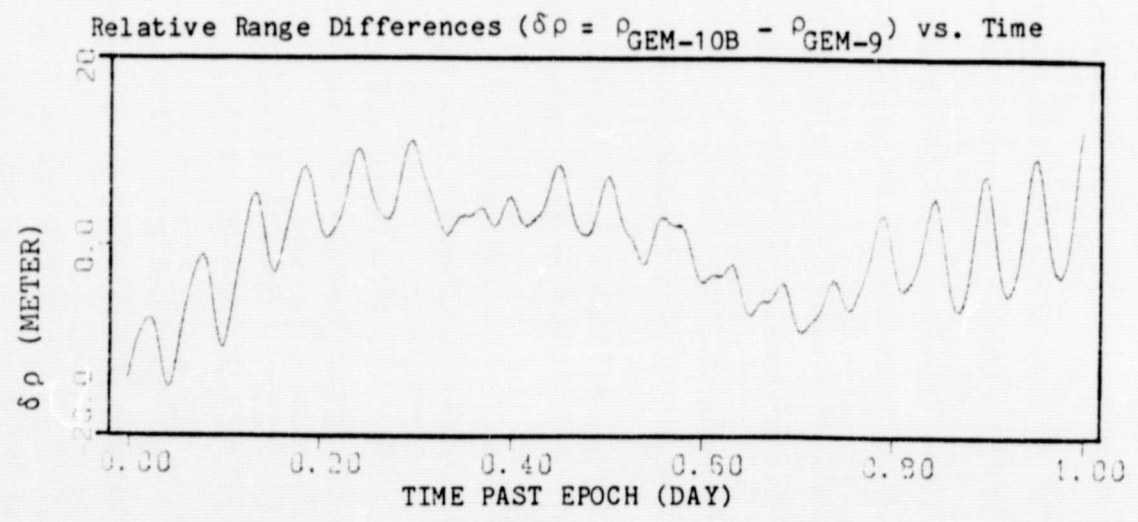Orbital Elements Used for each Model
Case C.4

Relative Range Differences ($\delta\rho = \rho_{GEM-10B} - \rho_{GEM-9}$) vs. Time

Figure 4.14b

Case C.3 (Continued)

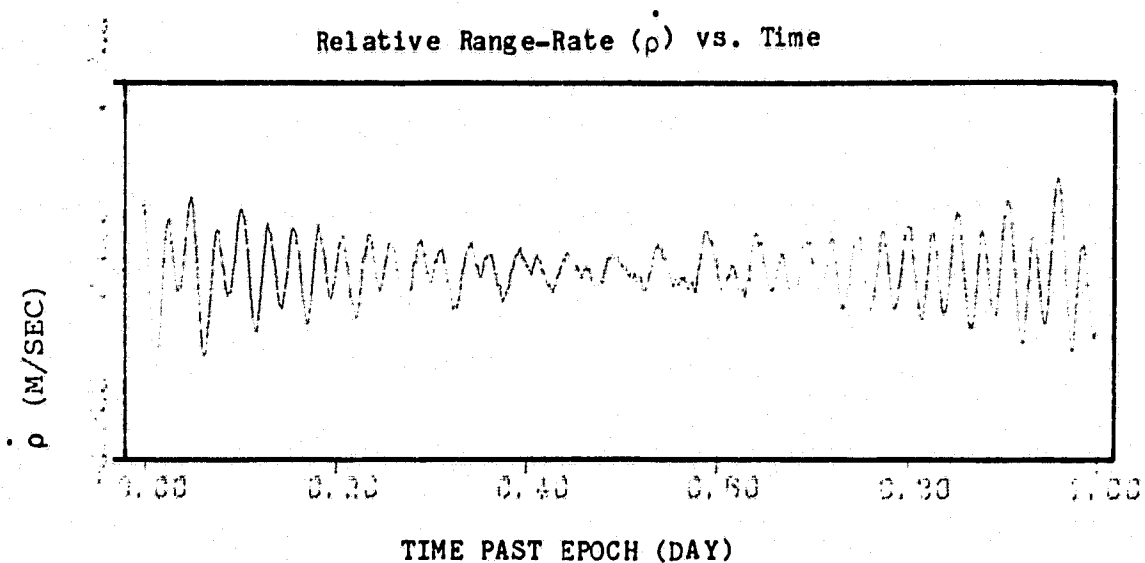Relative Range-Rate ($\dot{\rho}$) vs. Time

TIME PAST EPOCH (DAY)

Figure 4.15b

Case C.4 (Continued)

Relative Range-Rate Differences ($\delta\dot{\rho}$) vs. Time

$$\delta\dot{\rho} = \dot{\rho}_{GEM-10B} - \dot{\rho}_{GEM-9}$$

TIME PAST EPOCH (DAY)
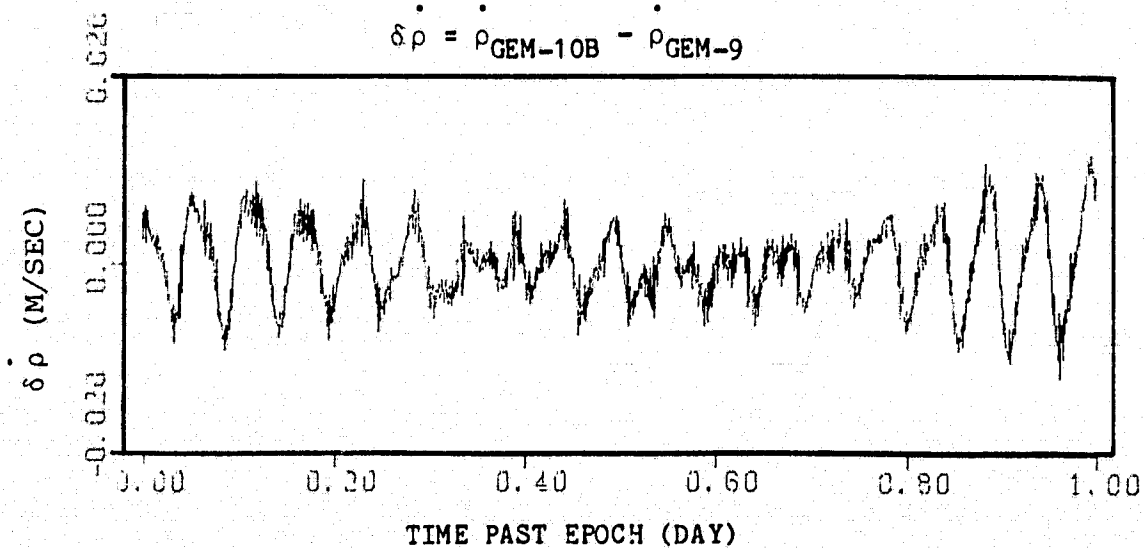
Figure 4.14c

Case C.3 (Continued)

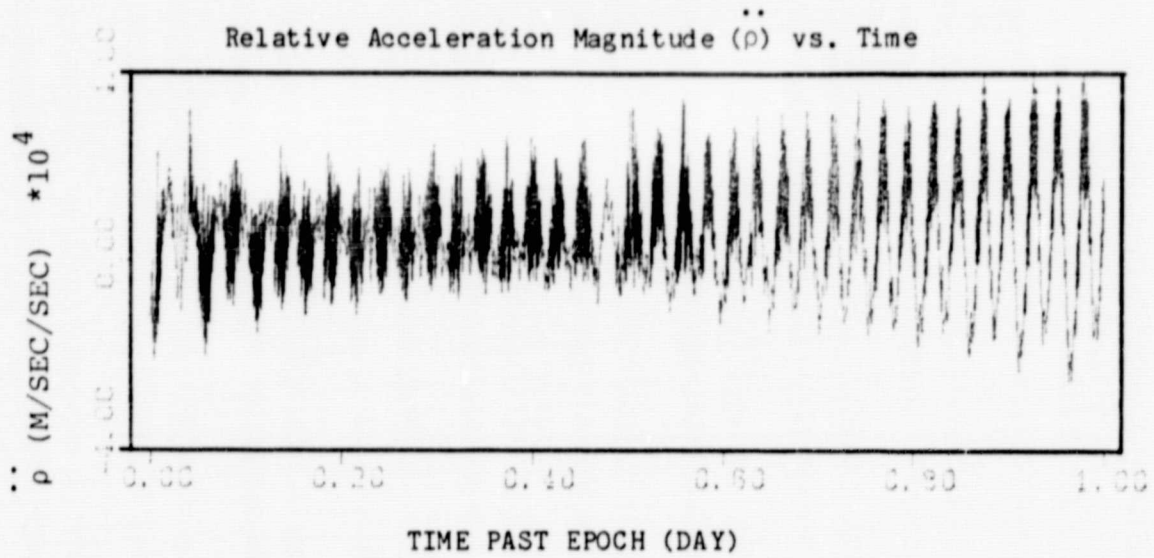Relative Acceleration Magnitude ($\ddot{\rho}$) vs. Time

TIME PAST EPOCH (DAY)

Figure 4.15c

Case C.4 (Continued)

Relative Acceleration Magnitude Differences ($\delta\ddot{\rho}$) vs. Time

$$\delta\ddot{\rho} = \ddot{\rho}_{GEM-10B} - \ddot{\rho}_{GEM-9}$$
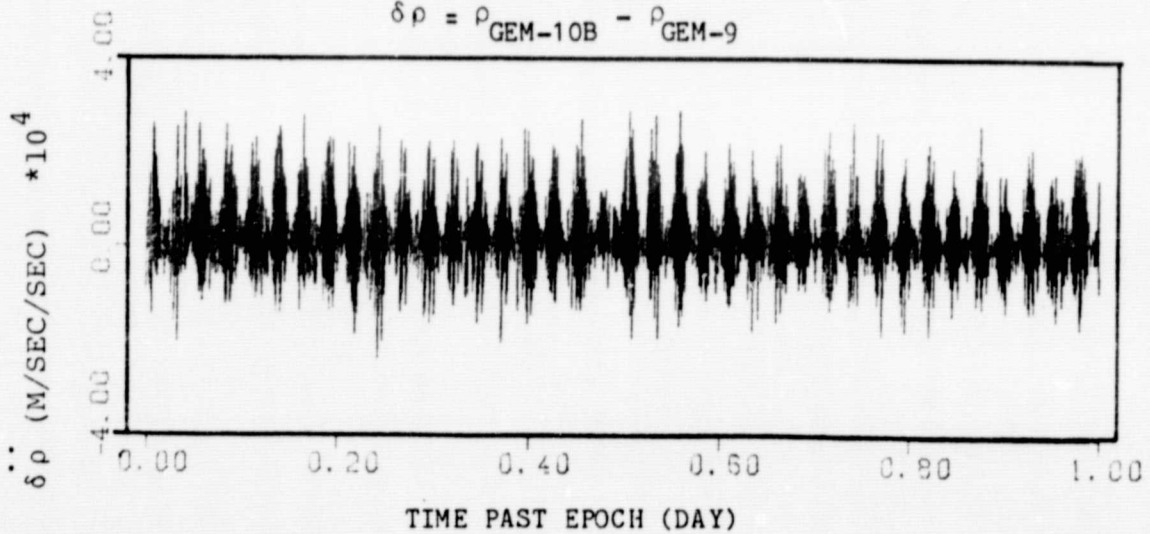

TIME PAST EPOCH (DAY)

Figure 4.16a

Prediction of the Relative Motions Characteristics for 6-Day
Arc Length with the Initial Orbital Elements of Case C.3
Gravity Model: GEM-9
Case C.5

Relative Range Variations from 300 km ($\Delta\rho$) vs. Time
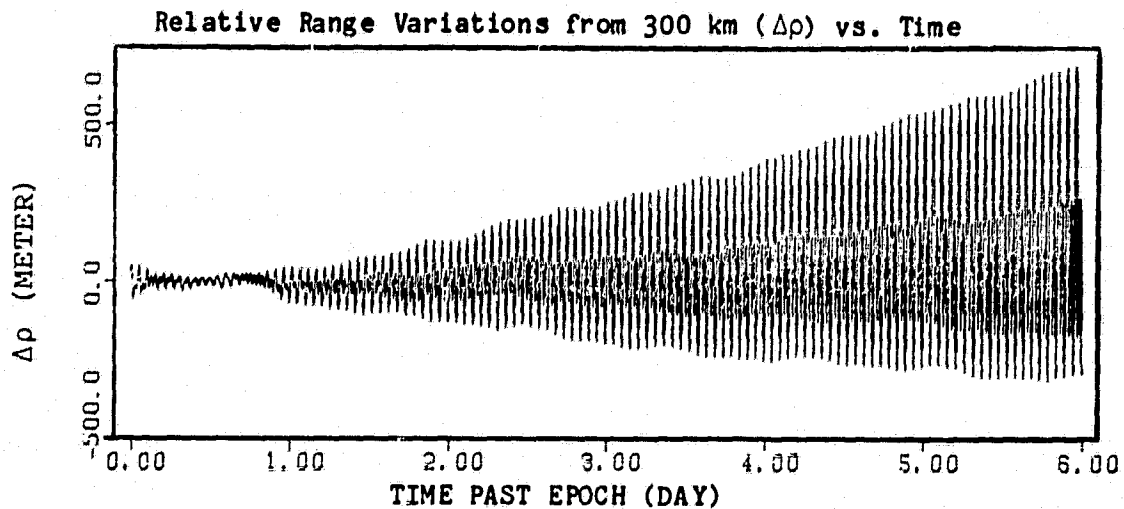

Figure 4.17a

Prediction of the Relative Motions Differences between
GEM-10B and GEM-9 Models for 6-Day Arc Length with
the Initial Orbital Elements of Case C.4
Case C.6

Relative Range Differences ($\delta\rho = \rho_{GEM-10B} - \rho_{GEM-9}$) vs. Time

Figure 4.16b
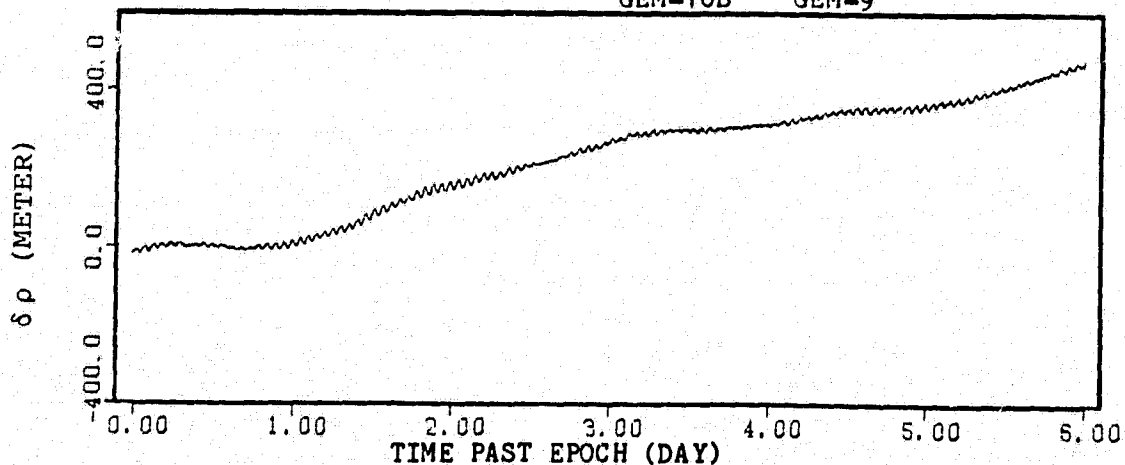
Case C.5 (Continued)

Relative Range-Rate ($\dot\rho$) vs. Time

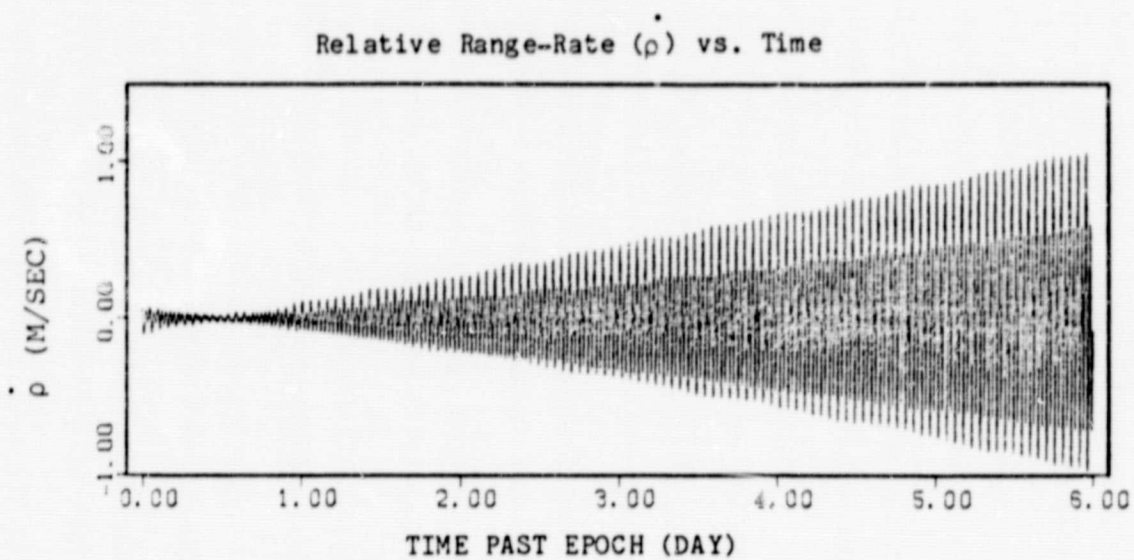

Figure 4.17b

Case C.6 (Continued)

Relative Range-Rate Differences ($\delta\dot\rho$) vs. Time

$$\delta\dot\rho = \dot\rho_{GEM-10B} - \dot\rho_{GEM-9}$$

Figure 4.16c

Case C.5 (Continued)

Relative Acceleration Magnitude ($\ddot{\rho}$) vs. Time

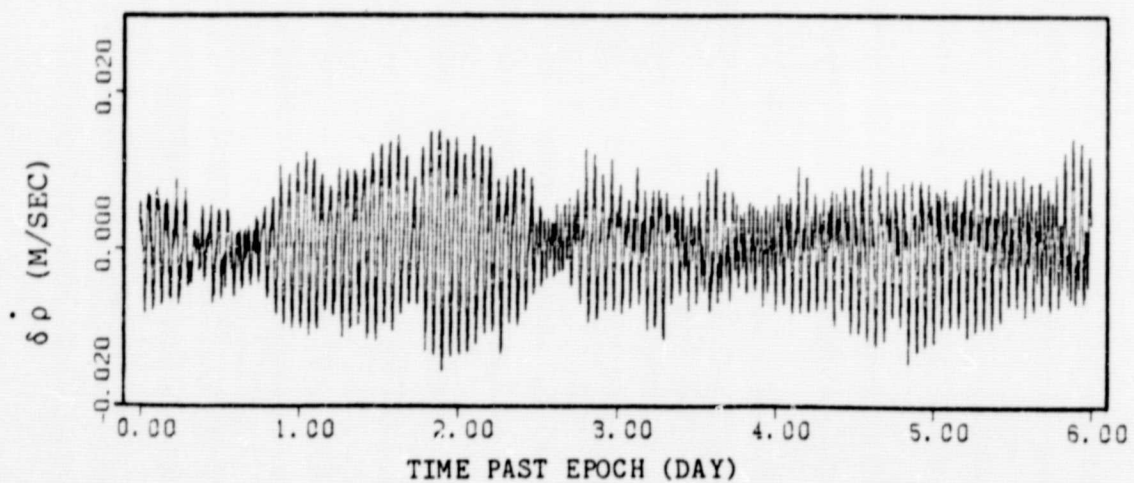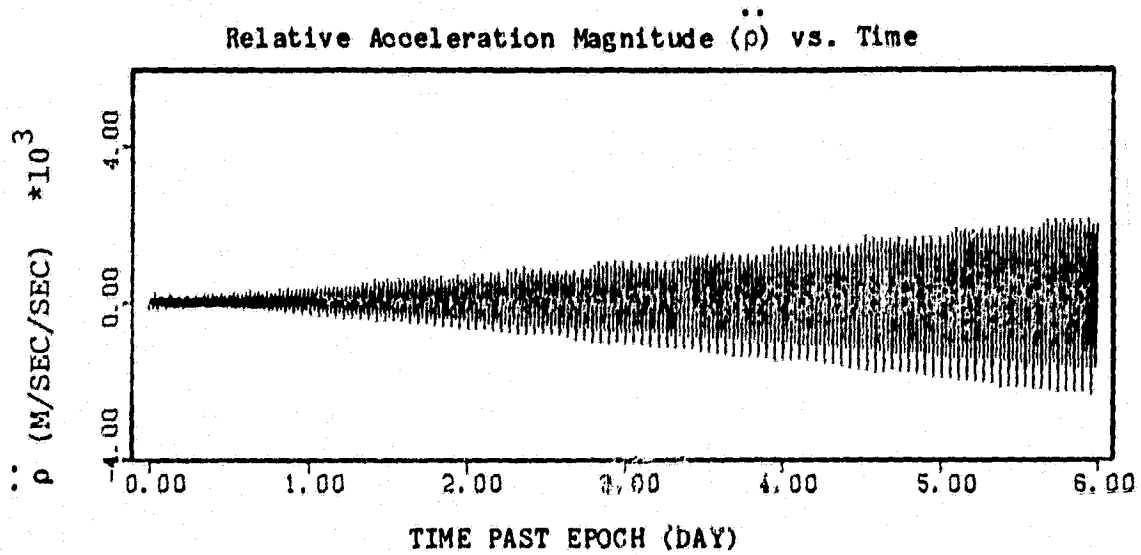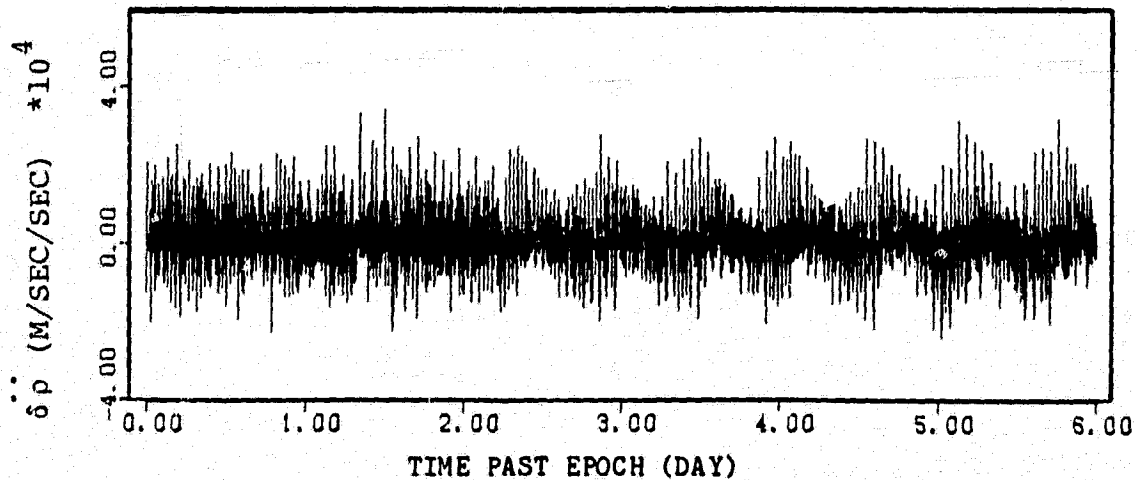TIME PAST EPOCH (DAY)

Figure 4.17c

Case C.6 (Continued)

Relative Acceleration Magnitude Differences ($\delta\ddot{\rho}$) vs. Time

$$\delta\ddot{\rho} = \ddot{\rho}_{GEM-10B} - \ddot{\rho}_{GEM-9}$$

TIME PAST EPOCH (DAY)

CHAPTER 5

CONCLUSIONS AND RECOMMENDATIONS

5.1 Summary

This preliminary study was conducted by performing numerous numerical experiments which provided the simulations of the relative motion characteristics between the two low altitude satellites. The simulations demonstrated the effects of two complete GEM-10B and GEM-9 gravity field models. Furthermore, there were various intervals of time (arc lengths) for which the simulations were generated.

Throughout the numerical experiments, the method which was developed in Chapter 3 was used to determine appropriate sets of initial orbital elements for the lead satellite whereas the initial orbital elements of the trailing satellite were held constant. The initial orbital elements of the lead satellite were obtained such that the two satellites would sense the same energy during the entire length of the simulation time. Consequently, in the generated simulations, only the minimum level of variations of the relative motions were demonstrated. In this manner, the ability of the method was well acknowledged in Chapter 4 wherein a maximum of 12-day simulation time was considered.

5.2 Conclusions

From the analysis of the numerical simulations provided in this investigation, the following conclusions can be made.

The simulations provided in Section 4.3 (Cases A.1 through A.8) demonstrated the fact that the stability of the system of two satellites is very sensitive to the initial orbital elements of the satellites. In the various cases which were considered, the stable behaviors were only possible to obtain with the appropriate selection of certain accurate set of initial orbital elements corresponding to the desired intervals of time. Moreover, it was also shown that the initial orbital elements obtained for an specified interval of time would not necessarily promise an stable behavior for a longer simulation time. In other words, an appropriate set of initial orbital elements were required in order to establish stability for the additional portion of the simulation time. Therefore, it can be concluded that in the actual mission it may be very difficult to hold the separation distance to small fluctuations; consequently, periodic adjustments to the orbits of the satellites may be required.

In addition, the simulations provided in Section 4.4 and 4.5 demonstrated the level of perturbations in the relative motions which were produced due to the effects of gravity field model error. Of course the level perturbations were also greatly reduced by the use of appropriate set of initial orbital elements which counteracted the effects of the error in the gravity field model.

C-2

Given that the GRAVSAT mission is expected to provide an accurate recovery of the geopotential model and that in the actual mission precise initial orbits for the satellites can not be practically achieved, it is essential that in the derivation of accurate observation equations (required for processing the actual data) which determine the quality and precision of the results, a considerable caution should be taken whenever a simplifying assumption is used or an approximation is made.

5.3 Recommendations

The following recommendations are suggested in order to improve the precision of the computed relative motions characteristics and the realism of the simulations.

The level of variations of the relative motions can be computed more accurately by converting the current single precision coded software program into double precision.

The only forces acting on the satellites considered in this study have been the central body gravitational forces. However, it is of importance to include the perturbations which will be produced due to other forces such as the effects of polar motion, direct and reflected solar radiation pressure and other non-gravitational forces. However, the drag compensation mechanism proposed for GRAVSAT should accommodate all surface forces, including radiation pressure. It should be noted that by including any of the above improvements the computer execution

time of the already considerable time consuming process will be increased.

It is suspected that the simulations of the components of the relative motions in the radial, transverse or along-track, and normal or cross-track directions can be more descriptive of the relative motion characteristics as compared with the simulations along the line of sight between the two satellites.

Finally, as mentioned previously, the simulations provided in this study were obtained with respect to an arbitrary set of initial orbital elements for the trailing satellite which, regardless of the various intervals of time, were held constant. However, it is suggested that for further studies these initial orbital elements be selected such that for any given interval of time and gravity field model, when the orbit of the trailing satellite is determined, it best fits the one in which only the two-body forces are modeled. This can be accomplished by using the same minimization method except that the constant separation distance should be set to zero. It is expected that the simulations of the relative motions obtained with the use of such initial orbital elements will demonstrate smoother behavior in the relative motions and that the fluctuations will be distributed more evenly along the simulation time.

REFERENCES

Brogan, W. L., _Modern Control Theory_, Quantum Publishers, Inc., New York, N. Y., 1974.

Colombo, O. L., _Global Geopotential Modelling from Satellite-to-Satellite Tracking_, Department of Geodetic Science and Surveying, the Ohio State University, Columbus, Ohio, Report No. 317, October 1981.

Forsythe, G. E., M. A. Malcolm, and C. B. Moler, _Computer Methods for Mathematical Computations_, Prentice-Hall, Inc., Englewood Cliffs, N. J., 1977.

Gaposchkin, E. M., "Global Gravity Field to Degree and Order 30 from Geos-3 Satellite Altimetry and other Data," _Journal of Geophysical Research_, Vol. 85, No. B12, pp. 7221-7234, December 1980.

Kaula, W. M., _Theory of Satellite Geodesy_, Blaisdell Publishing Company, Waltham, Massachusetts, 1966.

Kaula, W. M., "Inference of Variations in the Gravity Field from Satellite-to-Satellite Range-Rate," Department of Earth & Space Sciences, University of California, Los Angeles, California, December 1982.

Lerch, F. J., S. M. Klosko, R. E. Laubscher and C. A. Wagner, "Gravity Model Improvement Using Geos-3 (GEM-9 and 10)," _Journal of Geophysical Research_, Vol. 84, No. B8, pp. 3897-3915, 1979.

Lerch, F. J., C. A. Wagner, S. M. Klosko, R. P. Belott, R. E. Laubscher and W. A. Taylor, "Gravity Model Improvement Using Geos-3 Altimetry (GEM-10 and 10B)," _Marine Geodesy_, 1981.

Lundberg, J. B., "Multi-Step Integration Formulas for the Numerical Integration of the Satellite Problem," Institute for Advanced Study in Orbital Mechanics, the University of Texas at Austin, IASOM TR81-1, April 1981.

McKenzie, R. E. and K. Sepehrnoori, "Implementation of an Eighth-Order Runge-Kutta-Fehlberg Method," Institute for Advanced Study in Orbital Mechanics, the University of Texas at Austin, IASOM TR78-6, December 1978.

National Academy of Science (USA), Applications of a Dedicated Gravitational Satellite Mission, Report of the Workshop on a Dedicated Gravitational Satellite Mission, Washington, D.C., 1979.

Pisacane, V. L. and S. M. Yionoulis, Recovery of Gravity Variations from Satellite-to-Satellite Tracking, Applied Physics Laboratory, Johns Hopkins University, Baltimore, Report No. SDO-5583, 1980.

Pisacane, V. L., J. L. MacArthur, J. C. Ray, and S. E. Bergson-Willis, Description of the Dedicated Gravitational Satellite Mission (GRAVSAT), Int. Geosci. & Remote Sensing Symp., Washington, 1981.

Schutz, B. E. and B. D. Tapley, "UTOPIA: University of Texas Orbit Processor," Institute for Advanced Study in Orbital Mechanics, the University of Texas at Austin, IASOM TR80-1, 1980.

Shampine, L. F. and M. K. Gordon, Computer Solution of Ordinary Differential Equations, the Initial Value Problem, W. H. Freeman and Co., San Francisco, California, 1975.

Shao, R., Private Communication, 1982.

Tapley, B. D., "Statistical Orbit Determination Theory," Recent Advances in Dynamical Astronomy, Ed. by B. D. Tapley and V. Szebehely, D. Reidel Publishing Company, Dordrecht, Holland, pp. 396-425, 1973.

Wolff, M., "Direct Measurements of the Earth's Gravity Potential Using a Satellite Pair," Journal of Geophysical Research, Vol. 14, pp. 5295-5300, 1969.